THE ASTROPHYSICAL JOURNAL SUPPLEMENT SERIES, 124:265–283, 1999 September

QUASI-PERIODIC OSCILLATIONS IN BLACK HOLE CANDIDATES AS AN INDICATOR OF TRANSITION BETWEEN LOW AND HIGH STATES

ROBERT E. RUTLEDGE,[1,2] WALTER H. G. LEWIN,[3] MICHIEL VAN DER KLIS,[1,4] JAN VAN PARADIJS,[4,5] TADAYASU DOTANI,[6] BRIAN VAUGHAN,[2] TOMASO BELLONI,[4] TIM OOSTERBROEK,[7] AND CHRYSSA KOUVELIOTOU[8]

Received 1998 July 3; accepted 1999 February 23

ABSTRACT

By comparing positions on a spectral color-color diagram from 10 black hole candidates (BHCs) observed with *Ginga* (1354−64, 1826−24, 1630−47, LMC X-1, LMC X-3, GS 2000+25, GS 2023+33, GS 1124−68, Cyg X-1, and GX 339−4) with the observed broadband noise (BBN) (0.001–64 Hz) and quasi-periodic oscillation (QPO) variability, we find that the "very high state" is spectrally intermediate to the soft/high state and hard/low state. We find a transition point in spectral hardness where the dependence of the BHC QPO centroid frequency (of GS 1124−68 and GX 339−4) on spectral hardness switches from a correlation to an anticorrelation; where the BBN variability switches from high state to low state; and where the spectral hardness of the QPO relative to that of the BBN variability is a maximum. This coincidence of changing behavior in both the QPO and the broadband variability leads us to hypothesize that the QPO is due to interaction between the physical components which dominate the behaviors of BHCs when they occupy the hard/low and soft/high states. We conclude that these QPOs should be observed from BHCs during transition between these two states. Comparison with QPO and BBN behavior observed during the 1996 transition of Cyg X-1 supports this hypothesis. We also report 1-3 Hz QPOs observed in GS 2000+25 and Cyg X-1 in the hard/low state, and we compare these to the QPOs observed in GS 1124−68 and GX 339−4.

Subject headings: black hole physics — stars: individual (Cygnus X-1, GX 339−4, GS 1124−68) — stars: oscillations — X-rays: stars

1. INTRODUCTION

The X-ray (2–20 keV) phenomenology of galactic black hole candidates (BHCs) has been widely studied (see Tanaka & Lewin 1995 and van der Klis 1995 for recent reviews) and has stimulated much theoretical interest in the area (see Liang & Narayan 1997 for a recent review). The BHCs have many similarities in their phenomenology, in that similar X-ray spectral hardnesses are accompanied by similar fast-timing behavior (0.01–100 Hz). Often, it is this similarity of behavior alone which identifies an individual X-ray source as a BHC, when this source has no measured mass function, and it presents correlated X-ray spectral and timing behavior which is similar to that observed from BHCs which do have a (high, $\gtrsim 3\ M_\odot$) measured mass function.

This X-ray phenomenology is largely composed of three "states," historically tied to the observed source intensity, which has evolved to be tied to the source photon spectral hardness. The "soft/high" state (HS; historically, when the 1–10 keV source flux was high) is marked by a soft photon spectrum dominated by an "ultrasoft" blackbody component, with $kT \lesssim 1$ keV, and weak (∼few percent) root mean square (rms) variability which is a power law as a function of frequency, of slope ∼1. The "hard/low" state (LS) is marked by a hard photon spectrum dominated by a power-law component, and constant percent rms below some frequency (∼0.01–10 Hz), decreasing roughly as a power law above this frequency. The "very high" state (VHS) is marked by the presence of quasi-periodic oscillations (QPOs) with frequencies between 3–10 Hz. In addition, an "off" state (in which the source is quiescent) is generally included in any phenomenology. More recently, an "intermediate state" (IS; Belloni et al. 1996; Belloni et al. 1997; Méndez & van der Klis 1997) has been recognized, in which the variability is band limited, constant below some break frequency (∼0.1–10 Hz) and decreasing above this, while the energy spectrum shows both an ultrasoft blackbody component and a power-law component greater than 10 keV. The distinction made between this state and the HS and LS are the simultaneous presence of the ultrasoft and power-law energy spectral components, with band-limited broadband noise (BBN) variability and (in GS 1124−68) the presence of QPOs at source fluxes below that of the "high state."

As a structure for phenomenologically characterizing BHCs, the state paradigm lacks quantitative value. For example, Cyg X-1 may be observed in the HS. One might well ask, how high? Since "high" describes the observed flux, the uncertainty in distances to BHCs makes it difficult to intercompare the behavior of objects on this basis. There currently exists no gradation of states, no formal quantitative test to determine if a particular source occupies a state or not, or "how much" it occupies a state. The description of additional "states" without somehow tying them

[1] Department of Astronomy, University of California, Berkeley, CA 94720.
[2] Space Radiation Laboratory, MS 220-47, California Institute of Technology, Pasadena, CA 91125.
[3] 37-627, Dept. of Physics, Massachusetts Institute of Technology, Cambridge, MA 02139.
[4] Astronomical Institute "Anton Pannekoek," University of Amsterdam, Center for High Energy Astrophysics, Kruislaan 403, 1098 SJ Amsterdam, The Netherlands.
[5] Physics Department, University of Alabama in Huntsville, Huntsville AL 35899.
[6] Institute of Space and Astronautical Science, 3-1-1 Yoshinodai, Sagamihara Kanagawa 229-8510, Japan.
[7] Astrophysics Division, Space Science Department of ESA, ESTEC, P.O. Box 299, 2200 AG Noordwijk, The Netherlands.
[8] Universities Space Research Association, Huntsville, AL 35800.

through some invariant observational parameter to other "states" does not illuminate the relationship between the various states. In addition, it seems reasonable that the BHCs do not occupy "states" at all, but that BHC behavior changes slowly as a function of its observables, since individual BHCs are observed to have a wide range of luminosities, spectral hardnesses and power density spectra, rather than three or four of these. As such, investigating BHC behavior as a function of continual variables may be a useful observational approach.

In an individual source, observational states are defined on the basis of qualitative changes in its power spectrum and energy spectrum, which are observed to be strongly correlated. It seems likely that the instantaneous accretion rate ($\dot{M}$) is the underlying variable parameter responsible for the observed changes in source behavior. However, between different sources, other parameters—such as the mass of the black hole, or the stellar type of its companion—may also come into play in determining the observed source intensity behavior. Comparisons in behaviors between different objects therefore may eventually provide observational handles on these parameters.

The combined use of color-color diagrams (CCDs) and the contemporaneous timing behavior—usually indicated by the strength of source variability and its functional dependence on frequency in power density spectra (PDS)—has quite successfully revealed regularities in the complex QPO and BBN timing behavior of GS 1124−68 (Takizawa et al. 1997) and GX 339−4 (Miyamoto et al. 1991). Following this work, it was found that in the VHS, in which the QPOs are found, the PDS (apart from the QPOs) can be like those in the hard/low state, or like those in the HS (Miyamoto et al. 1993; Takizawa et al. 1997). In a similar vein, it has been shown that, as the fraction of the total intensity due to the power-law spectral component increases above 10%, the percent rms variability increases, as well (Miyamoto et al. 1994); the variability behavior of GS 1124−68 was demonstrated to be correlated to the strength of its hard spectral component, which had been long suspected.

The CCD versus fast-timing approach was first used in X-ray astronomy to untangle correlated timing and spectral/intensity behavior of nonpulsing neutron-star low-mass X-ray binaries (LMXBs; Hasinger & van der Klis 1989). Consequently, it has become clearer what the accretion rate is when the various distinct behaviors of these objects are observed. More detailed theory on the spectral and timing behavior has been produced, as well as proposals for the relationship between the behavior of neutron-star LMXBs and that of BHCs and pulsars (van der Klis 1994a, 1994b; see van der Klis 1995 for review).

We have completed a study of the simultaneous spectral and timing behavior of 10 BHCs observed with *Ginga* (1354−64, 1826−24, 1630−47, LMC X-1, LMC X-3, GS 2000+25, GS 2023+33, GS 1124−68, Cyg X-1, and GX 339−4). A description of BBN behavior of these sources is being presented elsewhere (Rutledge et al. 1999, hereafter BHCLFN). Here, we describe and discuss the spectral and energy dependence of QPOs in the four sources which exhibit them in the *Ginga* data (GS 1124−68, GX 339−4, Cyg X-1 and GS 2000+25) and the strength and frequency dependence of the underlying BBN. These results are a summary of analyses presented in greater detail elsewhere (Rutledge 1996).

We have examined the source spectral state, as characterized by its location on a CCD, and simultaneous timing properties. We find that BHCs show QPOs typically when they have a spectral hardness ratio between the hard/low state and soft/high state. When we follow the timing behavior of the two objects which exhibit this QPO (GX 339−4 and GS 1124−68) as a function of spectral hardness, changes in behavior of the QPO and the underlying BBN indicate that the so-called VHS is a transition between the LS and the HS. This has important implications for the origin of the QPO, as an indicator of this transition, perhaps being produced by interaction between two distinct physical processes responsible for the HS and LS phenomena.

An important note on terminology: Historically, "low state" was applied to describe the behavior of BHCs when the source intensity was low, and "high state" for when it was high. We are faced with a descriptive problem, in that the behavior of the BHCs we describe herein—aside from intensity, and the presence of QPO—is indistinguishable from that observed from the "low state," or the "high state." It is a common aspect of theories of BHC accretion to ascribe the low state to one physical component, such as a geometrically thick accretion disk or a spherical corona, and the high state behavior to another, such as a geometrically thin accretion disk (e.g., Narayan & Yi 1994; Abramowicz, Chen, & Taam 1995; Narayan & Yi 1995; Chen et al. 1995; Chen & Taam 1996; Narayan 1996; Esin, McClintock, &Narayan 1997). Therefore, throughout this paper we use the terms "low state" and "high state" not to indicate source intensity, but behavior which is ascribed to the respective physical components we mention above.

2. THE X-RAY DATA AND ANALYSES

All X-ray data on black hole candidates (BHCs) in the present work were obtained with the Large Area Counter (LAC) on the *Ginga* satellite (Turner et al. 1989). The LAC on board *Ginga* had a geometric area of $\sim$4000 cm^2, a nominal energy range of 1–37 keV, divided into 48 energy channels, with energy resolution of 18% $(E/6\ \mathrm{keV})^{1/2}$. The time resolution of the data, depending on the data-acquisition mode, was typically between 0.001 and 16 s.

2.1. *Color-Color Diagram*

The data used in the CCD are described in detail elsewhere (BHCLFN; Appendix B in Rutledge 1996). Briefly, our data are drawn from all data acquired by *Ginga* during observations of each of 10 X-ray black hole candidates (1354−64, 1826−24, 1630−47, LMC X-1, LMC X-3, GS 2000+25, GS 2023+33, GS 1124−68, Cyg X-1, and GX 339−4), which had energy resolution sufficient to produce our hardness ratios (see also below). All data were corrected for background, dead time, and aspect. Following these corrections, we produced hardness ratios using three bands—the low-energy range (2.3–4.6 keV), the medium-energy range (4.6–9.2 keV) and the high-energy range (9.2–18.4 keV). These bands were combined into the hard ratio (high-energy range/medium-energy range) and the wide ratio (high-energy range/low-energy range), which we use to produce the CCD. Each point represents 128 s of contiguous integration time. Only points which have error bars in both colors showing significantly measured hardness ratios ($>4\ \sigma$) are shown (the remainder are discarded). Due to inadequate background subtraction, not all data acquired

TABLE 1

QUANTITY OF BHC DATA FOR TIMING ANALYSIS, BY SOURCE AND TEMPORAL RESOLUTION

	Time Resolution				
Source	0.00781 s (ks)	0.06250 s (ks)	0.5000 s (ks)	>0.5 s (ks)	Total (ks)
Cyg X-1	25.2	4.2	1.9	55.8	87.0
GS 1124−68.....	54.6	57.9	268.4	0.0	380.8
GS 2000+25.....	30.7	9.4	27.1	71.2	138.3
GX 339−4.....	15.2	23.0	15.2	18.9	72.4

by *Ginga* on a particular source is used in this CCD. Thus, the CCD is biased against fainter intensities, for which either the background subtraction techniques employed or counting statistics in a 128 s integration were inadequate. After all selections were applied, a total of 680 ks (of 1500 ks) of data from all sources were used in the CCD. The CCD is presented in § 3.1.

In the lowest energy bin, the effect of galactic absorption is minimized (although not eliminated) by using a high lower energy bound (2.3 keV). All BHCs in the present study have column densities between 1.4×10^{21} cm^{-2} and 6.0×10^{21} cm^{-2}, except GS 2000+25 (8.4×10^{21} cm^{-2}) and 1630−47 (25×10^{21} cm^{-2}; van Paradijs 1995). The effect of galactic absorption in the 2.3–4.6 keV energy range is small—for a blackbody of $kT = 0.5$ keV, the wide ratio changes by less than 10% between 1.4×10^{21} cm^{-2} and 6.0×10^{21} cm^{-2}; at 25×10^{21} cm^{-2}, this becomes a 30% effect in the 2.3–4.6 keV energy range.

Throughout the present work, we refer to spectral "states," typically as indicated by the contemporaneous wide ratio value. For brevity, we use a progression of letters (A, B, C, D, ..., J) which indicate a range of wide ratio space, each half a decade wide in logarithmic space, increasing in sequence with increasingly hard spectrum (A is $-4.0 \leq$ wide ratio ≤ -3.5, B is $-3.5 \leq$ wide ratio ≤ -3.0, etc.). The width of these ranges was arbitrarily chosen, with the idea that the source behavior does not vary significantly within a single range. This is not always the case, particularly when QPOs are observed, and it then becomes necessary to further subdivide the data based on the spectral values into "substates" (e.g., F1, F2, ...). However, the letters A–J are retained for convenience in referencing the timing analysis to a simultaneous spectral indicator.

2.2. *Timing Analysis*

In Table 1, we show the quantity of data which are available to us for the timing study, separated by source and time resolution. In all, 853 ks are available for the fast-timing analysis; of this, 305 ks have time resolution of or better than 0.06250 s.

An extensive description of our PDS production, including mathematical definitions, normalization, and computation of correction factors for dead time and background, is to be found elsewhere (Rutledge 1996). We repeat the pertinent details here.

2.2.1. *Composite PDS*

To make efficient use of all available data, each observation was used to produce any (or all) of three possible types of FFTs, which we define here:

Low-frequency FFT.—Data are binned to 16.0 s, with a total duration of 1024 s, using 64 bins of data. The resulting frequency range is 0.0009765–0.03125 Hz.

Medium-frequency FFT.—Data are binned to 0.0625 s, with a total duration of 64 s, using 1024 bins of data. The resulting frequency range is 0.015625–8 Hz.

High-frequency FFT.—Data are binned to 7.8125 ms, with a total duration of 8 s, using 1024 bins of data. The resulting frequency range is 0.125–64 Hz.

Thus, a single observation with a duration of 1500 s and a time resolution of 7.8 ms is used to produce 187 high-frequency FFTs, 23 medium-frequency FFTs and 1 low-frequency FFT.

Using raw data selected from those listed in Table 1 (listed in greater detail in Appendix B of Rutledge 1996), we produced FFTs in three separate energy bands: the low-energy range (=2.3–4.6 keV), medium-energy range (=4.6–9.2 keV), high-energy range (=9.2–18.4 keV) and in the summed intensity range (=2.3–18.4 keV). This produced a library of low-, medium-, and high-frequency FFTs in three independent photon energy ranges and one summed photon energy range from which we draw to produce PDS, based on the selection criteria we apply for any given analysis.

To produce a composite PDS, individual FFTs are selected by the wide ratio, measured during the time period covered by the FFT. Each individual FFT is made into a single PDS, its calculated dead-time–corrected Poisson level subtracted, and the resulting power corrected for background and instrumental dead time. Finally, all the resulting PDS are averaged together into a single PDS. The uncertainty in the power at each frequency is taken to be the measured standard deviation in the power divided by the square root of the number of measurements. Thus, the uncertainty in the power contains any (nonbiased) systematic uncertainty in the Poisson-subtraction, dead time, and background percent rms correction factors.

These PDS are logarithmically rebinned, and overlapping frequency ranges are dropped in the PDS with the lesser integrated time. For example: with 50 medium-frequency FFTs and 200 high-frequency FFTs, the medium-frequency FFTs represent 64 s × 50 = 3200 s of data, while the high-frequency FFTs represent 8 s × 200 = 1600 s of data. Therefore, all the data less than 8 Hz would be dropped in the high-frequency PDS, and then the two PDS are merged.

The final frequency range of the composite PDS is 0.00097–64 Hz or less if data of sufficient contiguous duration or time resolution are not available, and it is normalized as rms^2 Hz^{-1} and corrected for dead time and background.

The data of the high-, medium-, and low-frequency range parts of the single PDS are not necessarily taken at the same time. Thus, this type of PDS is subject to systematic uncertainties due to changes in the PDS within a single selection criteria. In addition, there may be more data available in one frequency range than in others.

For each of the 10 individual objects, we produced four composite PDS (of the low-, medium-, and high-energy range, and for the full intensity range) from data selected by wide ratio to be in each of the coarse spectral hardness bins (A, B, C, ...), as illustrated in Figure 1 and described in § 3.1. We used these PDS to investigate the dependence of BBN variability on spectral hardness, to search for the presence of QPOs and understand the dependence of QPO properties on spectral hardness and photon energy.

There are, at times, intensity "spikes" that occur in the data, a few ms in duration, which are typically not due to source variability, but instead to a variety of background sources (some of these spikes were due to geomagnetically trapped particles from orbiting nuclear power generators. These events, and the observed 2–37 keV PHA spectra, are discussed further elsewhere [Rutledge 1996]). We systematically excluded these spikes from our analysis, as they can produce significant, measurable power across all frequencies. When a single time bin is found in which the number of counts is 20 σ (calculated from the intrinsic

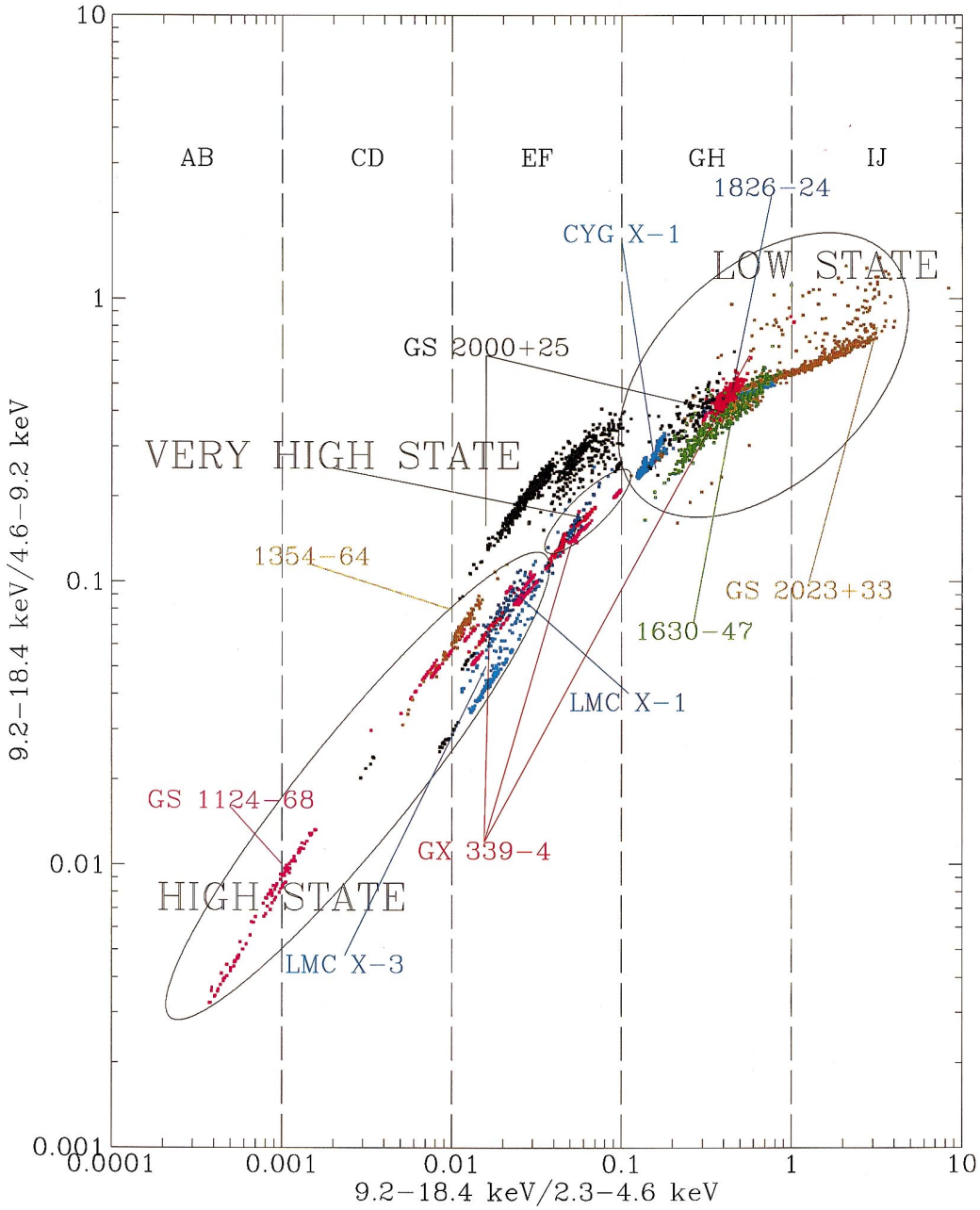

FIG. 1.—Color-color diagram. A composite color-color diagram of all 10 BHC sources observed by *Ginga* (1354−64, 1826−24, 1630−47, LMC X-1, LMC X-3, GS 2000+25, GS 2023+33, GS 1124−68, Cyg X-1, and GX 339−4), which shows the range of spectral hardness observed from each source. Data have been corrected for background counts as well as for aspect and dead time, prior to producing the hardness ratios. Each point represents 128 s integration. Only values of the hardness ratio which are more than 4 σ significant are shown.

scatter of the data used for that particular FFT) greater than the mean number of counts, that value was replaced by a value randomly selected from a set of bins in the data used for that FFT. Such events, even if real, are identifiable as discrete events, which are not our primary focus.

2.3. *Parameterized Fits to the PDS*

In practice, the models adopted to fit a PDS may not be ideal, or even formally acceptable according to statistical tests. Discrepancies may be systematic—for example, due to the skew of a quasi-Lorentzian peak which is not accounted for in the model—or they may be due to excursions from simply parameterizable continuum behavior in the PDS—that is, deviations from the model which are nonbiased, like random scatter, but statistically significant. There exists no a priori reason that such biased and noisy PDS should not exist. Thus, while it is desirable to fit the models as closely to the data as possible, there can be a trade-off between the accuracy and simplicity of a model. These parameterizations are not physically motivated, and thus their utility is to accurately describe PDS using a small set of numbers.

For the present study, we desire simple parameterizations which adequately describe PDS from all 10 sources. We avoid the introduction of new parameters, apart from switching to a more reasonable parameterization. We use a maximum-likelihood fitting method (least χ^2; Press et al. 1995), and quote the 1 σ single parameter uncertainties, the reduced χ^2, and the number of degrees of freedom.

We use a number of models, most of which have become widely used in describing PDS of X-ray binaries, to fit the observed power (P) as a function of frequency (ν) to the PDS. The model shapes we used to fit to the real source variability are all continuous functions of frequency and include the following:

1. Power law, $P \propto \nu^{-\alpha_1}$.
2. Flat-top single power law, a constant power below some frequency ν_1 breaking to a power law with slope α_1 above this frequency.
3. Broken power law, represented by one power-law slope (α_1) below a critical frequency ν_1 and a different, typically steeper, power law with slope α_2. If we find $\alpha_1 \lesssim 0.3$ (that is, if the first power law is very flat), then we call this model "flat-top single power law" instead of a "broken power law." This is a definition of convenience, having no theoretical or observational impetus.
4. Flat-top broken power law, a constant power below some frequency ν_1 breaking to a power law with slope α_1 above this frequency, breaking again to a (typically steeper) power law α_2 above frequency ν_2, with $\nu_1 < \nu_2$.
5. Double flat-top single power law, a model in which the power is constant below some frequency ν_1, breaking to a power law of slope α_1, which evens out into a constant value again at some higher frequency ν_2 ($>\nu_1$), and then breaks again into a power law of the same slope (α_1) at some higher frequency ν_3.
6. Flat-top power-law exponential, a model in which the power is constant below some frequency ν_1, and continuous with the product of a power law and an exponential function above this frequency.

In fitting models to the data, we employ one of the above models, which we call the continuum model, or Broadband noise (BBN) model, and a model to account for quasi-periodic oscillations from:

1. Lorentzian, used to model quasi-periodic oscillations, which has a centroid frequency ν_c and full width at half-maximum (FWHM; Γ), and a normalization related to the percent rms variability.
2. Harmonics, sometimes added to account for the appearance of harmonics and sub-harmonics to the QPO; the frequencies and FWHM values of these harmonics are constrained to be 0.25, 0.5, 2.0 and 4.0 that of the Fundamental, except where noted.

The percent rms variability of the Lorentzians and harmonics are integrated between $-\infty$ and ∞ Hz.

2.4. *Energy Dependency of the PDS*

We present the results of the fits to the four sources in which we observed QPOs (GS 1124−68, GX 339−4, Cyg X-1, and GS 2000+25) in four energy ranges. For each PDS, we indicate the mean source spectrum by the wide ratio (=high-energy range/medium-energy range). Finally, we fitted the PDS with BBN and QPO models to determine the parameterization of the PDS and the percent rms variability in each spectral state.

3. RESULTS

3.1. *Color-Color Diagram*

In Figure 1, we show a color-color diagram (CCD) of all X-ray data in the present study, showing the wide ratio versus the hard ratio.

The dashed-line divisions on the figure are artificial boundaries, separating the spectral parameter space into equally sized areas based on the wide ratio. These divisions are labeled with the alphabetic shorthand (A, B, C, D, etc.), encompassing two such ranges, corresponding to a decade in magnitude of the wide ratio.

The approximate locations of each source are labeled on the CCD. The CCD shows that, for most of these sources, spectral evolution in these colors produces roughly parallel tracts which run diagonally across the CCD. These tracks show smooth variation in the spectrum within the CCD, although there are discontinuities—likely due in part to short observing times relative to the timescale of spectral evolution.

We have approximately indicated the positions on the CCD where BBN behavior expected from the various "states" was observed in the PDS of sources in that area. Sources which are spectrally soft, have PDS which have a single–power-law dependence on frequency, and present only weak (~few percent rms) variability (1–20 keV) occupy the area labeled "high state." Sources which are spectrally hard, have complex PDS—typically, but not always, constant below a frequency ~0.1–10 Hz, and decreasing as a power-law at higher frequencies—and have strong (~20%–50% rms) variability (1–20 keV) occupy the area labeled "low state." The behavior of high-state and low-state variability will be presented in detail elsewhere (BHCLFN). Sources which present QPO occupy the spectral range labeled "very high state."

Some sources were only observed to occupy the low state (such as GS 2023+33, 1630−47, 1826−24, and Cyg X-1). Others were observed only in the high state (1354−64 and

LMC X-3). Some were observed to traverse two or more of these states (GS 1124−68, GX 339−4, and LMC X-1—although the observation of LMC X-1 in the spectral region corresponding to the VHS did not have sufficient time resolution to confirm the presence of QPOs).

In Figure 2, we show on the same scale as Figure 1 the points at which QPOs were identified (by eye) as present in the PDS of several sources in the present study. In addition, we include a point from QPO from GX 339−4 in a previous study (Grebenev et al. 1991), observed with the ART-P spectrometer, with a centroid frequency of 0.8 Hz, FWHM of 0.15 Hz, and a percent rms variability of $7.0 \pm 0.8\%$ in the 3–25 keV energy range. When this QPO was detected from GX 339−4, the energy spectrum was power law, with a photon slope of 1.733 ± 0.004. This places GX 339−4 at (wide ratio, hard ratio) vector of (0.32, 0.40), found by propogating the observed photon spectral model through the *Ginga* response (see § 3.1.1). While the wide ratio of the sources in the present study span four orders of magnitude, the QPO is largely clustered within less than 1 order of magnitude, located close to a single locus in the CCD. Sources which were observed to exhibit QPO were also observed at other times at different positions on the CCD, but with no QPOs.

Figure 3 shows the wide ratio for each of the 10 sources (same data as Fig. 1, described above). There are three

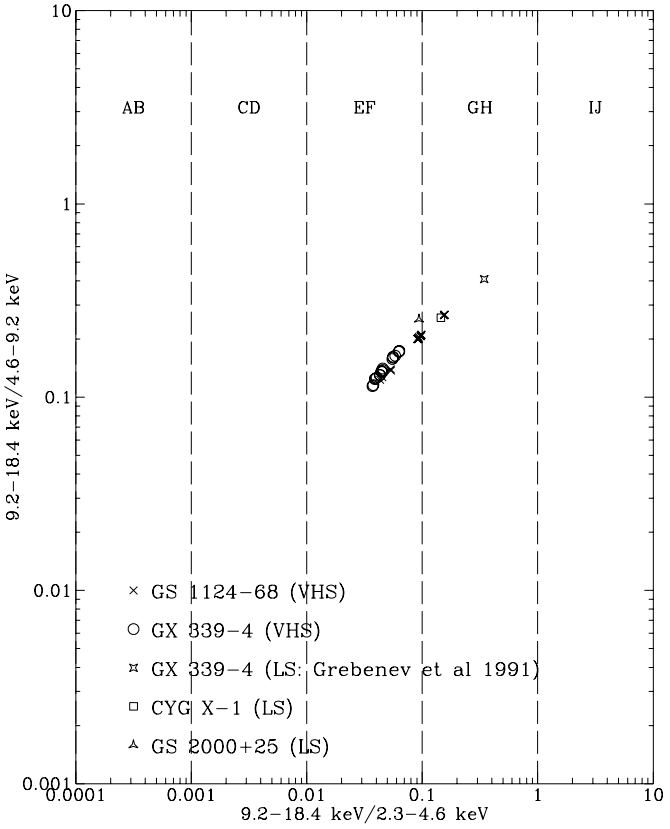

FIG. 2.—Very high state and low state QPOs, Located on the wide ratio vs. hard ratio CCD. The position on the wide ratio vs. hard ratio CCD, when QPO is observed from GS 1124−68 (VHS), GX 339−4 (VHS and low state from Grebenev et al. 1991), Cyg X-1 (low state), and GS 2000+25 (low state). For clarity, only a few representative points for each source are shown. This figure may be directly compared with the full composite CCD in Fig. 1. While the black hole candidates occupy four orders of magnitude in wide ratio parameter space, the QPOs are observed largely within one order of magnitude in wide ratio.

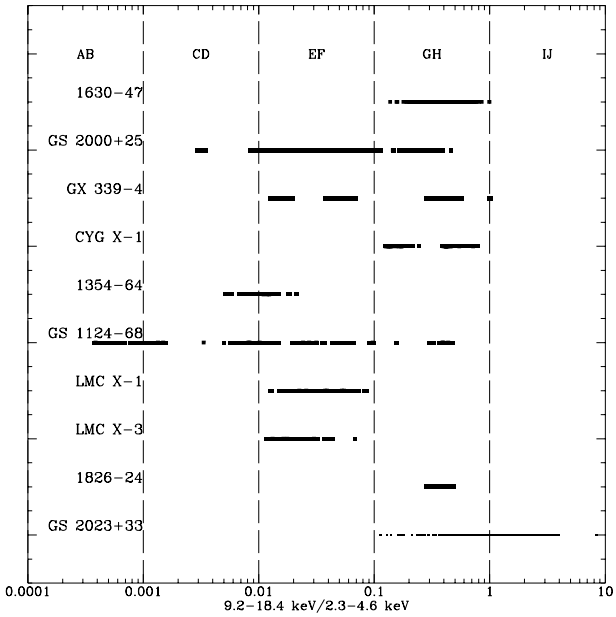

FIG. 3.—Source hardness ratios. The wide ratio of all 10 BHC sources in the present study, which shows the range of spectral hardness observed from each source. Each point represents 128 s integration.

sources—GS 2000+25, LMC X-1, and LMC X-3—in which some observed wide ratio values are similar to those observed from GX 339−4 and GS 1124−68 when 3–10 Hz QPOs were observed (the VHS spectral range). Timing analysis of all observations (but one) of GS 2000+25 produced upper limits to QPO strength well above that observed from GX 339−4 and GS 1124−68; in the one observation near wide ratio = 0.1 (at the edge of the VHS spectral range), 2.6 Hz QPO from GS 2000+25 was observed (see § 3.2.4). LMC X-1 and LMC X-3 were observed with time-resolution of 16 s—too long to measure QPO at 3–10 Hz. Thus, we do not observe any BHCs which exhibit spectral hardness in the VHS spectral range, but no QPO (with upper limits below the observed strengths in GX 339−4 and GS 1124−68).

3.1.1. *Intrinsic Source Spectrum to Wide Ratio Conversion*

As the wide ratio (as measured by *Ginga*) is the parameter to which we tie the observed behavior, we provide a figure to relate this ratio to the observed photon spectral parameters of a power law, blackbody, and the relative strength of the two. To do so, we simulated photon energy spectra with blackbody temperatures of $kT = 0.1$, 0.25, 0.4, 0.55, 0.7, 0.85, 1.0, and 1.4 keV; with photon power-law spectra of slopes 0.9, 1.3, 1.7. 2.1, 2.5, and 2.9. (We use the blackbody spectrum as a simple parameterization, although more physically reasonable models, such as a disk blackbody spectrum, may more accurately describe the spectrum in this energy range; Mitsuda et al. 1984; Makishima et al. 1986). We combined these two spectral components with different relative strengths, indicated by the ratio (X) of 2–20 keV photon flux (photons s^{-1}) of the power law to that of the blackbody, for values of X in the range of 0.0001–100.

The relationships between X and wide ratio for these assumed photon spectra are shown in Figure 4. To have a wide ratio of $\lesssim 0.01$, a BHC must be dominated by the blackbody (that is, ultrasoft) component. To obtain a wide

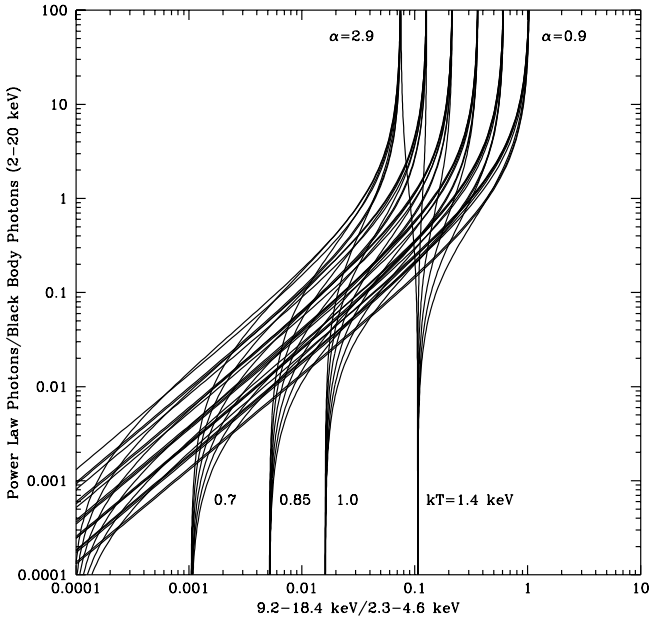

FIG. 4.—Intrinsic source energy spectrum vs. wide ratio. The intrinsic source photon spectrum is indicated by a combination of the ratio of the power-law photon flux to the blackbody photon flux (2–20 keV), the photon power-law slope ($\alpha = 0.9$–2.9, spaced by 0.4), and the blackbody temperature (0.1, 0.25, 0.4, 0.55, 0.7, 0.85, 1.0, and 1.4 keV). The wide ratio is obtained by folding the intrinsic source photon spectrum through the *Ginga* LAC response matrix.

ratio of $\gtrsim 0.1$, BHCs with photon spectral slopes less than 2.2 must be dominated by the power-law photon spectral component. At steeper spectral slopes, and in between 0.01–0.1 where most of the QPO in GS 1124−68 and GX 339−4 are observed, the wide ratio is a complex function of X, kT, and the photon spectral power-law slope.

3.2. *Power Density Spectra*

Here, we present the parameters describing the QPOs and their energy dependence, including the strength of the simultaneously observed BB variability and the models used to describe them. The detailed results pertaining to BBN variability when QPOs are not observed, and the detailed parameters and energy dependence of the BBN variability when QPOs are observed are presented elsewhere (BHCLFN; Rutledge 1996).

3.2.1. *Cyg X-1*

Of the measured wide ratio values for Cyg X-1, 80% were in the range 0.13–0.51, which is within the low state described in § 2.1.

When Cyg X-1 exhibited QPOs, the values of its wide ratio are largely in one of two ranges: 0.12–0.15 and 0.16–0.18. These in turn correspond to two different observational periods (90/129–131 and 91/156–157, respectively). We subdivided these data into two spectral groups: wide ratio = 0.1–0.15 (G1), and 0.15–0.32 (G2). The QPO parameters from the best-fit models are given in Table 2.

In Figure 5, we show the PDS of the G1 and G2 spectral ranges, with the power renormalized as νP. For all energy ranges, the PDS are identical above 10 Hz. Below 10 Hz, the PDS are different and appear to be complex functions of frequency. Most evident is the presence of a QPO peak near 1 Hz in the PDS of the G1 data. The best-fit BBN variability model, without a QPO Lorentzian near ~ 1 Hz, has a $\chi^2_\nu > 13$, which decreases to ~ 1.6 when the Lorentzian is added. The percent rms variability of this QPO decreases with increasing energy range from 11.7 ± 0.5 in the low-energy range to 8.2 ± 0.6 in the high-energy range.

We also fitted a Lorentzian to the G2-data PDS. In the intensity range a peak was found at 3.14 Hz, with FWHM 0.7 ± 0.3 Hz. These values were fixed for the low-energy range, medium-energy range, and high-energy range PDS, in which the percent rms was consistent with being colorless.

This QPO peak is very broad ($Q \sim 1$), which would usually result in its being called a "noise" feature, as QPO is a term traditionally reserved for higher Q signals. We attempted to distinguish this feature from the QPO of GX 339−4 and GS 1124−68 (see § 3.4) based on the QPO spectral hardness as a function of the source photon spectral hardness but found we were unable to do so on this basis. We therefore forward the hypothesis that this feature is related to the QPO observed in the data from GS 1124−68 and GX 339−4.

3.2.2. *GX 339−4*

Of the measured wide ratio values for GX 339−4, 80% were in the range wide ratio = 0.044–0.56.

We closely examined the data obtained in the 1988 September observations of GX 339−4, divided by source spectrum, which is the only period during which the wide ratio was in the F spectral range, and during which the VHS QPO was observed. In Figure 6, we show the wide ratio as a

TABLE 2

QPO PARAMETERS FOR BEST-FIT CYGNUS X-1 COMPOSITE PDS

Spectral Range (Wide Ratio)	Energy Range (keV)	ν_c (Hz)	FWHM (Hz)	rms (%)
G1[a]	2.3–4.6	1.07 ± 0.04	1.30 ± 0.09	11.7 ± 0.5
(0.1–0.15)	4.6–9.2	1.15 ± 0.03	1.04 ± 0.08	10.1 ± 0.4
	9.2–18.4	1.14 ± 0.03	0.8 ± 0.1	8.2 ± 0.6
	2.3–18.4	1.11 ± 0.03	1.17 ± 0.07	10.8 ± 0.4
G2[b]	2.3–4.6	(3.14)	(0.72)	$3.5^{+0.3}_{-0.4}$
(0.15–0.32).....	4.6–9.2	(3.14)	(0.72)	$3.3^{+0.5}_{-0.6}$
	9.2–18.4	(3.14)	(0.72)	<6.0
	2.3–18.4	$3.14^{+0.09}_{-0.07}$	0.7 ± 0.3	$3.5^{+0.3}_{-0.4}$

NOTE.—Values in parenthesis are fixed Upper limits are 3 σ.

[a] Fits applied to values in the 0.001–64 Hz range.

[b] Fits applied to values in the 0.0156–64 Hz range.

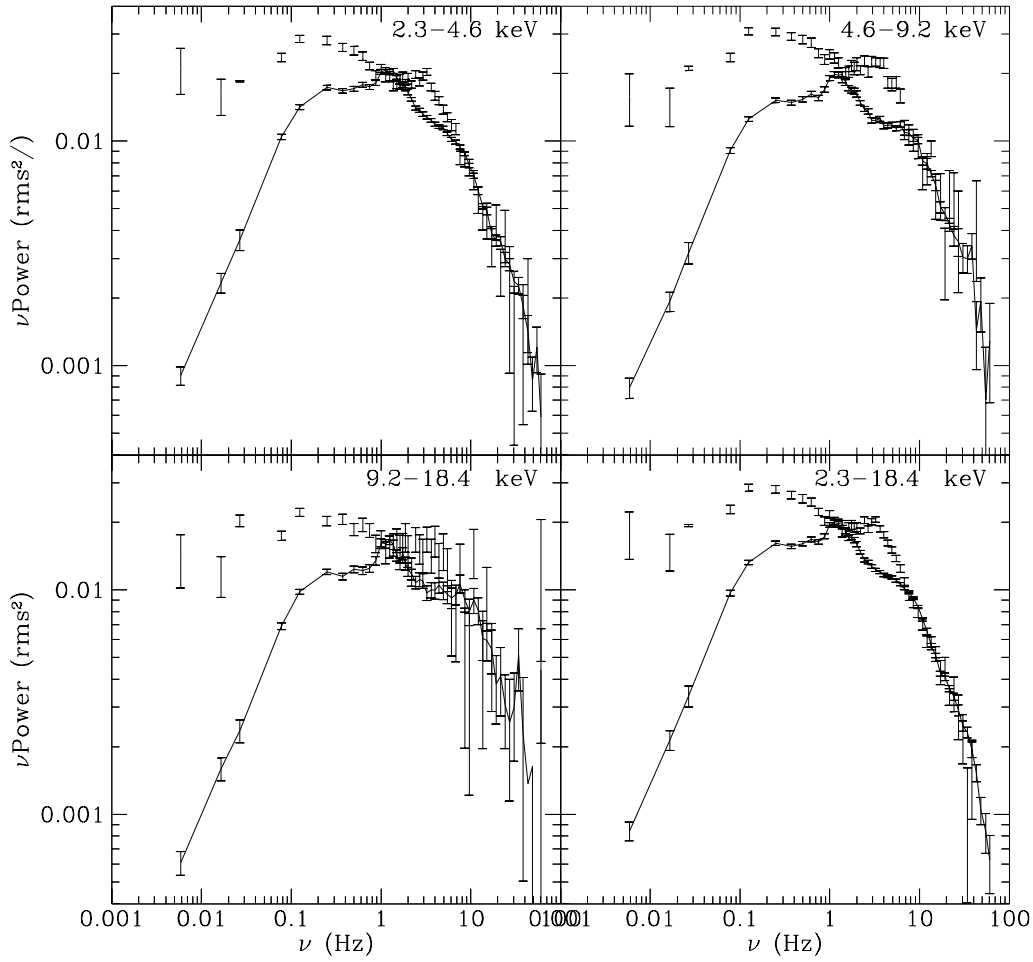

FIG. 5.—Cyg X-1 composite PDS, G1 and G2. Eight PDS of Cyg X-1, in four energy ranges (indicated in each panel). There are two PDS for each energy range: one from data taken when the source wide ratio is in the range 0.1–0.15 (G1; *connected by a line to guide the eye*), and one from data taken when the source wide ratio is in the range 0.15–0.32 (G2, *unconnected points*). The 1 σ error bars are included. The spectrally soft PDS shows a QPO feature near 1 Hz, while the harder PDS does not have this feature. The PDS show roughly equal percent rms values above 10 Hz, and percent rms values which are not equal below 10 Hz.

function of time during these observations. The source spectrum (measured by wide ratio) hardens between $t = 0$ and 2 days; over the next 2 days, the source spectrum globally softens, while exhibiting short-term reversals—variously hardening and softening.

We divided the data by spectrum and labeled the spectral regions (F1–4; all in the F-state) on the hardness-intensity diagram (HID) in the upper right panel of Figure 6. We recognize at least three separate tracks in the HID—a nearly constant count-rate track (near $I = 5800$ counts s^{-1} 2.3–18.4 keV, crossing the regions labeled "F3" and "F4"), a nearly constant wide ratio track (near wide ratio = 0.045—labeled as "F2"), and a steeply sloped track (the wide ratio region labeled "F1"). These tracks correspond to those found in Figure 5 of Miyamoto et al. (1991) and Figure 5.28 of Ebisawa (1991).

We used the medium-frequency and high-frequency FFTs in each spectral region to produce composite PDS, in all energy ranges. We show these PDS in Figure 6, in the bottom 16 panels. The scale of all PDS is given in the bottom left panel. When spectrally hardest (F3 and F4), the source shows band-limited noise, breaking at a frequency of $\approx$few Hz, in addition to QPO which is strongest in the 9.2–18.4 keV energy band. When spectrally softer (F1 and F2), the PDS show less variability, and a frequency dependence which is more like a power law, or perhaps band-limited with a break frequency near 0.02 Hz.

We fitted the composite PDS produced from the F1–4 data of GX 339−4. The models used were single power law (for F1), double flat-top single power law (for F2, with the low-frequency flat-top ν_1 frozen to below 0.01 Hz), and flat-top single power law (states F3 and F4). For all these, we also fitted harmonic QPOs, allowing the percent rms normalization in the first two harmonics and subharmonics to vary. Typically, the high-energy range PDS did not constrain the models well; for these PDS, we froze the BBN model parameters (except the percent rms) at their best-fit values found from the intensity range PDS.

In Table 3, we list the QPO and BBN percent rms values found from these fits. In all PDS, the strength of QPOs increases with increasing photon energy. The strength of the QPO does not show a monotonic dependence on spectral hardness of GX 339−4. Looking at the PDS, one might be misled to believe that the percent rms of the QPO in the low-energy range PDS increases with increasing spectral hardness; our model fits do not bear this out. One is appar-

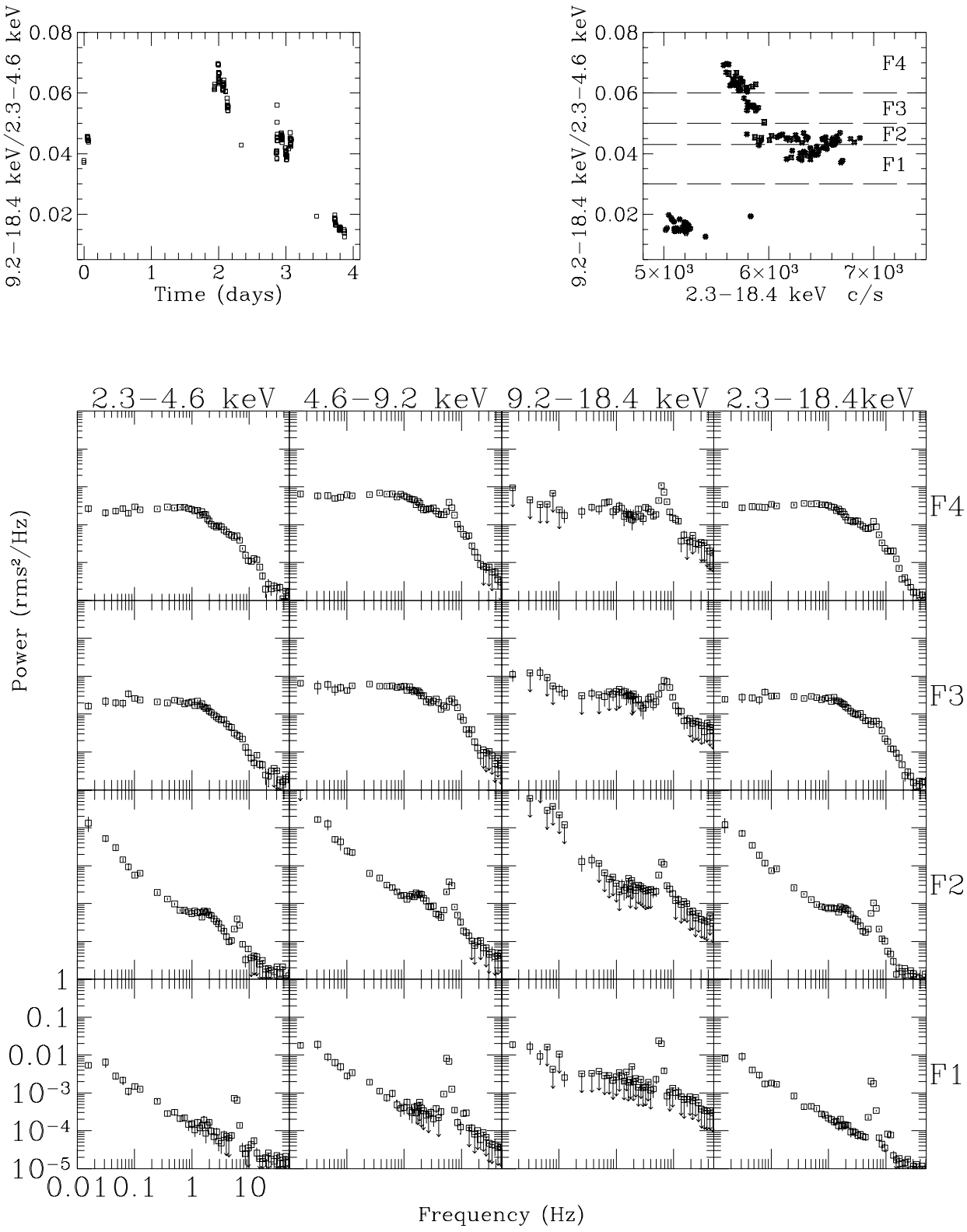

FIG. 6.—Detailed HID and PDS of GX 339−4 with QPOs. Each column is headed with the energy range of the data used for those PDS, and each row is labeled according to spectrum, corresponding to the divisions in the HID at the top of the figure. (*Upper left panel*) Wide ratio vs. time, during the period in which QPOs were observed from GX 339−4 (1988 September; time = 0 is 88/247 13:37 UT). (*Upper right panel*) HID, intensity range count rate vs. wide ratio during the 1988 September observation. The panel has been divided by wide ratio value, and each region is labeled. (*Bottom panels*) PDS in three energy ranges plus the intensity range (labeled by column) of the 1988 September observations. Upper limits are 2 σ. The data were divided by spectral hardness (each row is labeled, and corresponds to a label in the HID above). The BBN PDS characteristics evolve—as the spectrum softens, the BB PDS changes from a flat-top power law to a pure power law, while the QPO remains throughout.

TABLE 3

PERCENT RMS OF QPO AND BBN IN GX 339−4

Wide Ratio	Energy Range (keV)	QPO rms (%)	BBN rms (0.001–64 Hz) (%)	BBN model	FWHM (Hz)	ν_c (Hz)	χ^2_ν (dof)
0.030–0.043.....	2.3–4.6	1.79 ± 0.04	3.89 ± 0.09	PL	0.53 ± 0.03	5.80 ± 0.02	1.36 (139)
(F1)	4.6–9.2	5.97 ± 0.08	6.3 ± 0.2	PL	0.53 ± 0.02	5.80 ± 0.01	1.87 (139)
	9.2–18.4	10.5 ± 0.2	5.6 ± 0.5	PL	0.55 ± 0.03	5.78 ± 0.01	1.36 (140)
	2.3–18.4	2.89 ± 0.04	4.45 ± 0.07	PL	0.47 ± 0.02	5.80 ± 0.01	2.42 (139)
0.043–0.050.....	2.3–4.6	$2.29^{+0.3}_{-0.08}$	13.5 ± 0.8	DFTPL	$0.59^{+0.2}_{-0.3}$	6.40 ± 0.04	2.25 (46)
(F2)	4.6–9.2	8.7 ± 0.1	23.3 ± 1.5	DFTPL	1.07 ± 0.06	6.37 ± 0.02	2.60 (46)
	9.2–18.4	17.4 ± 0.4	24.3 ± 2	DFTPL	1.4 ± 0.1	6.42 ± 0.04	1.58 (49)
	2.3–18.4	4.24 ± 0.06	15.4 ± 0.7	DFTPL	0.95 ± 0.05	6.36 ± 0.02	4.28 (46)
0.050–0.060.....	2.3–4.6	1.1 ± 0.2	8.4 ± 0.2	FTPL	(3.58)	(6.9)	1.13 (48)
(F3)	4.6–9.2	5.7 ± 0.1	13.0 ± 0.2	FTPL	3.17 ± 0.2	7.08 ± 0.07	1.43 (47)
	9.2–18.4	11.5 ± 0.4	8.9 ± 0.7	FTPL	3.55 ± 0.3	7.38 ± 0.09	1.05 (48)
	2.3–18.4	2.7 ± 0.1	9.5 ± 0.1	FTPL	3.40 ± 0.3	6.9 ± 0.1	1.39 (46)
0.060–0.075.....	2.3–4.6	1.85 ± 0.06	8.8 ± 0.1	FTPL	(2.27)	(6.27)	2.73 (47)
(F4)	4.6–9.2	5.9 ± 0.1	13.2 ± 0.3	FTPL	2.35 ± 0.1	6.38 ± 0.03	2.12 (45)
	9.2–18.4	9.3 ± 0.2	8.0 ± 0.4	FTPL	1.80 ± 0.1	6.39 ± 0.04	2.30 (47)
	2.3–18.4	3.24 ± 0.05	9.6 ± 0.1	FTPL	2.37 ± 0.09	6.27 ± 0.03	2.71 (45)

NOTE.—Fits applied to values in the 0.125–64 Hz range.

ently misled by the relative strength of the BBN power, which accounts for a dominant portion of the percent rms at the QPO frequency when the spectrum is hard, but considerably less when the spectrum is soft. While we do see dependence between the QPO percent rms in the low-energy range it is not monotonic, nor pronounced, with the percent rms values in the range of 1.1%–2.9%.

The QPO FWHM and centroid frequency exhibit some dependency (again, nonmonotonic) on spectral hardness. In the intensity range the FWHM increases from 0.5, to 1.0, to 3.6, and back down to 2.3 as the spectrum hardens between states F1–4. The centroid frequency goes from 5.8, to 6.3, to 7.4, to 6.3 as the spectrum hardens between states F1–4. In all states, the QPO parameters (centroid frequency, FWHM) are energy independent.

3.2.3. *GS 1124−68*

Of the measured wide ratio values for GS 1124−68, 80% were in the range 0.00098–0.38, which is within the low state described in § 2.1.

The QPO properties in the summed 1.2–18.4 keV range exhibited by GS 1124−68 have been examined in detail (Takizawa et al. 1997, hereafter T97). We here reexamine these properties in our three energy ranges, as well as the intensity range, using the wide ratio spectral indicator.

Over short periods of time (∼hours) there is typically very little evolution in the source spectral hardness, less than 0.5 dex in hardness ratio (see T97, BHCLFN). We therefore produced PDS over single observational epochs. We adopted the same time periods used by T97, and the same labels for these time periods (by number 1–15), with two exceptions: (1) we did not distinguish between observation 5L and 5H (where "L" stands for periods within the trough of a "flip-flop"—see T97 for a description of this phenomenon), while "H" stands for the elevated count-rate periods around the flip-flop—they are joined under the single header "5"; also, we split observation 11 into 11a and 11b. The time limits for the data used here are listed in Table 4, along with the frequency range of the resultant PDS, and the mean wide ratio for each observation period. The uncertainty listed in the wide ratio is the 1 σ spread of observed 128 s values (the relatively small values demonstrate that the amount of spectral evolution during a single observational epoch is typically small).

As found previously (T97 and references therein; Belloni et al. 1997), QPO is detected during observations 1, 2, 3, 5, 10, 11, and 15. The QPO during observation 11 appears is strongest in the second half (11b).

In Table 5, we list the centroid frequency, FWHM, and percent rms of the fundamental QPO in each PDS in which QPO was identified by T97. In addition, we find (weak) QPO in observations 8 and 11a. The fundamental was identified for each observation as that QPO peak with the greatest percent rms in the 9.2–18.4 keV range, or, if none are identified, in the 4.6–9.2 keV range.

The QPO was fitted as a series of harmonics, with frequencies and FWHM values which are factors of 0.25, 0.5, 1.0, 2.0, and 4.0 of those of the fundamental. Typically, only the subharmonic at 0.5 ν_c and the second harmonic at 2 ν_c were invoked (permitting the best-fit value of the percent rms in each to be determined). For a few, however, three or four harmonics have significant percent rms values. These harmonics were studied in detail elsewhere (T97; Belloni et al. 1997; Rutledge 1996).

In all cases, the percent rms of the fundamental increases with increasing photon energy (except observation 15, where the S/N is too low to permit detection in the high-energy range).

In addition to the detailed parametric fits to the PDS of the individual observations, we also produced PDS using the F1–4 division done for GX 339−4, for qualitative comparison with that source. These are shown in Figure 7, produced similarly as for GX 339−4 (see Fig. 6). When the source is spectrally hard (F3 and F4), the PDS show band-limited noise with a break frequency of a few Hz, along with QPO which is strongest in the 9.2–18.4 keV energy band. When the source is spectrally soft (F1 and F2), the PDS shows weaker variability and a frequency dependence which is either power-law (F2) or band-limited noise with a break frequency of ≈0.1 Hz. This behavior is similar to that observed from GX 339−4 using the same spectral hardness division.

TABLE 4

DIVISION OF GS 1124−68 DATA

Observation ID	Start Time (UT)	End Time (UT)	PDS Frequency Range	⟨Wide Ratio⟩
1	91/011 00:51	01:17	0.0156–8.0 Hz	0.155 ± 0.004
2	91/011 19:37	20:42	0.0156–8.0	0.097 ± 0.006
3	91/011 20:49	91/012 00:05	0.0156–64.0	0.092 ± 0.003
4 (not used).....	...	...	...	...
5	91/014 19:48	23:25	0.0156–8.0	0.054 ± 0.004
6	91/016 18:46	23:27	0.0156–8.0	0.026 ± 0.005
7	91/017 18:05	21:57	0.0156–8.0	0.014 ± 0.001
8	91/018 17:30	21:27	0.0156–8.0	0.024 ± 0.003
9	91/020 15:17	17:15	0.0156–8.0	0.027 ± 0.001
10.....	91/022 17:18	20:09	0.0156–64.0	0.058 ± 0.004
11a	91/025 12:48	13:10	0.0156–64.0	0.036 ± 0.001
11b	91/025 13:46	13:56	0.0156–64.0	0.044 ± 0.001
12.....	91/036 10:34	11:07	0.0156–64.0	0.027 ± 0.002
13.....	91/037 10:05	12:13	0.0156–64.0	0.029 ± 0.001
14.....	91/044 05:04	08:38	0.0156–8.0	0.024 ± 0.004
15.....	91/045 06:11	08:10	0.0156–64.0	0.013 ± 0.001
16.....	91/051 23:29	91/053 04:32	0.0156–64.0	0.0093 ± 0.0017
17.....	91/056 20:56	91/058 00:19	0.0156–64.0	0.0068 ± 0.0007
18.....	91/067 14:28	91/109 20:13	0.0156–64.0	0.0009 ± 0.0007
19.....	91/137 03:12	91/204 21:04	0.0156–64.0	0.3995 ± 0.1578

3.2.4. *GS 2000+25*

Of the measured wide ratio values for GS 2000+25, 80% were in the range 0.021–0.23. The values of the hard ratio are typically higher than those observed for other objects with similar wide ratio values.

In a check of PDS of individual observation periods, a period of significant variability was found on day 252 of 1988 (September 8, ∼140 days into the outburst), between 15:45 and 17:24 UT. During this period, the source was in a spectral state with wide ratio = 0.09–0.1. We show the PDS, from an average of 44 medium-frequency FFTs, in Figure 8. We fitted the data with a flat-top power-law function with an additional Lorentzian component to account for QPO near 2 Hz. We find that the QPO component is required by the data in the low-energy range (compare $\chi^2_\nu = 3.4$ for 29 degrees of freedom, or dof, without the QPO component to 0.7 for 26 dof with the QPO component). We fitted the flat-top single power law plus QPO model to the low-energy range, medium-energy range, and high-energy range PDS made from data taken during the period when the LS QPO was observed. The best-fit model parameters are listed in Table 6. The centroid frequency (intensity range PDS) is 2.63 ± 0.06, FWHM is 1.7 ± 0.2, and the percent rms variability is consistent with being independent of energy.

We produced a PDS using data with a wide ratio consistent with that observed from GS 1124−68 and GX 339−4 while they exhibit VHS QPO (F range). Visual inspection of the PDS from this observation finds no QPO peak. After finding the best-fit BBN models in the intensity range we added a Lorentzian, with $\nu_c = 4$, 5, and separately 6 Hz, with FWHM = 1.0 Hz, to obtain 3 σ upper limits of the percent rms variability of such components, which were 7.2%, 4.8%, and 7.5% (respectively). In the high-energy range the corresponding 3 σ upper limits were 29%, 26%, and 30%. As these limits are greater than the measured strength of VHS QPO in GX 339−4 and GS 1124−68, we cannot exclude the presence of VHS QPO in these data.

3.3. *The Energy Dependence of the QPO*

In Figure 9, we show the centroid frequency and FWHM of the QPO in GX 339−4 and GS 1124−68 as a function of spectral hardness. In both GX 339−4 and GS 1124−68, the centroid frequency is dependent on spectral hardness. The centroid frequency is greatest near wide ratio = 0.055 (±0.01 approximately) and decreases as the source becomes spectrally harder and as the source becomes spectrally softer. The same is true for the FWHM of the QPO—it is greatest at wide ratio = 0.055 and smaller as the source is spectrally harder or softer. We also include the QPO of Cyg X-1 and GS 2000+25 in this figure, which show roughly consistent behavior.

In Figure 10, we show the percent rms variability as a function of photon energy for QPO and BBN variability in GS 1124−68 and GX 339−4. In both GS 1124−68 and GX 339−4 (Figs. 10*a* and 10*d*), the VHS QPO percent rms (averaged over all observations) increases with increasing energy. The BBN average power (Figs. 10*b* and 10*e*), however, increases from the low-energy range to the medium-energy range ; it then remains constant or decreases between the medium-energy range and high-energy range.

In GS 1124−68, when there is no QPO observed (Fig. 10*c*), the BBN average power increases with increasing photon energy across all three energy ranges. To produce this panel, we used observations 6, 7, 9, 12, and 14, in which VHS QPOs were not observed, but the source spectrum was similar to that during times when VHS QPOs were observed (in the range 0.01–0.03 vs. 0.013–0.155). In the low-energy range and medium-energy range the average broadband power is considerably larger when QPO is present than when QPO is absent (compare 9.8 ± 0.1% and 18.3 ± 0.5% rms with 2.8 ± 0.05% and 10.0 ± 0.2% rms). However, in the high-energy range, the average power is comparable (15.4 ± 0.8% rms with QPOs, 17.1 ± 0.4% rms without). The average ratio of BBN variability in the high-energy range versus the low-energy range when QPO is

TABLE 5

GS 1124−68 QPO FUNDAMENTAL PARAMETERS

Observation ID	Energy Range (keV)	ν_c (Hz)	FWHM (Hz)	rms (%)	χ^2_ν (dof)
1.....	2.3–4.6	3.004 ± 0.008	0.37 ± 0.1	2.4 ± 0.1	1.61 (39)
	4.6–9.2	2.98 ± 0.01	0.36 ± 0.05	4.9 ± 0.2	1.24 (39)
	9.2–18.4	3.004 ± 0.008	0.29 ± 0.05	7.0 ± 0.1	2.46 (39)
	2.3–18.4	2.98 ± 0.001	0.50 ± 0.06	4.0 ± 0.1	1.24 (39)
2.....	2.3–4.6	5.02 ± 0.05	1.02 ± 0.2	1.6 ± 0.2	1.20 (41)
	4.6–9.2	5.07 ± 0.02	0.80 ± 0.04	4.8 ± 0.1	1.99 (43)
	9.2–18.4	5.02 ± 0.02	0.69 ± 0.04	7.9 ± 0.2	1.99 (43)
	2.3–18.4	5.03 ± 0.02	0.83 ± 0.05	2.86 ± 0.08	1.80 (41)
3.....	2.3–4.6	5.33 ± 0.02	0.97 ± 0.06	1.74 ± 0.05	1.33 (500)
	4.6–9.2	5.325 ± 0.008	0.69 ± 0.03	5.4 ± 0.1	1.34 (500)
	9.2–18.4	5.33 ± 0.009	0.74 ± 0.03	10.6 ± 0.1	1.32 (509)
	2.3–18.4	5.329 ± 0.007	0.82 ± 0.03	3.19 ± 0.05	1.80 (501)
5.....	2.3–4.6	(7.38)	(2.46)	<0.80	1.56 (43)
	4.6–9.2	6.82 ± 0.09	$1.7^{+0.4}_{-0.6}$	2.4 ± 0.4	1.64 (41)
	9.2–18.4	(7.38)	(2.46)	9.2 ± 0.2	1.97 (46)
	2.3–18.4	7.4 ± 0.1	2.45 ± 0.3	1.3 ± 0.14	2.29 (41)
8.....	2.3–4.6	(5.65)	(2.2)	0.9 ± 0.07	1.65 (47)
	4.6–9.2	(5.65)	(2.2)	2.7 ± 0.1	1.95 (47)
	9.2–18.4	(5.65)	(2.2)	8.8 ± 0.6	2.00 (47)
	2.3–18.4	5.65 ± 0.15	$2.2^{+0.9}_{-0.6}$	1.0 ± 0.04	0.99 (42)
10	2.3–4.6	(7.72)	(3.7)	0.7 ± 0.1	1.64 (46)
	4.6–9.2	8.11 ± 0.05	3.9 ± 0.2	6.0 ± 0.3	1.68 (44)
	9.2–18.4	8.43 ± 0.03	3.27 ± 0.08	16.4 ± 0.2	1.73 (45)
	2.3–18.4	7.72 ± 0.04	3.7 ± 0.1	2.55 ± 0.06	2.27 (44)
11a	2.3–4.6	(7.5)	(2.11)	<0.36	1.27 (52)
	4.6–9.2	(7.5)	(2.11)	1.4 ± 0.2	1.75 (50)
	9.2–18.4	(7.5)	(2.11)	<5.1	0.76 (52)
	2.3–18.4	7.8 ± 0.3	2.11 ± 0.6	0.56 ± 0.07	2.55 (52)
11b	2.3–4.6	(5.82)	(0.35)	1.10 ± 0.08	1.47 (48)
	4.6–9.2	5.816 ± 0.009	0.33 ± 0.08	$8.0^{+0.8}_{-0.4}$	1.06 (46)
	9.2–18.4	5.81 ± 0.01	0.36 ± 0.15	15.7^{+3}_{-1}	0.72 (47)
	2.3–18.4	5.813 ± 0.008	0.36 ± 0.07	3.2 ± 0.3	1.36 (46)
15	2.3–4.6	4.5 ± 0.1	$1.3^{+0.3}_{-0.2}$	0.67 ± 0.05	1.20 (46)
	4.6–9.2	4.83 ± 0.09	$1.1^{+0.3}_{-0.2}$	1.6 ± 0.2	1.22 (39)
	9.2–18.4	(4.68)	(1.14)	<4.8	1.58 (51)
	2.3–18.4	4.68 ± 0.04	0.96 ± 0.14	0.75 ± 0.04	1.36 (39)

NOTES.—Frequency ranges used to fit and wide ratio are in Table 4. Values in parenthesis are fixed Upper limits are 3 σ.

absent is 6.1 ± 0.2 versus only 1.6 ± 0.1 when QPO is present. This may imply that the presence of QPO suppresses BBN variability in the high-energy range.

In Figure 11 we show the energy dependence of the LS QPO in Cyg X-1 and GS 2000+25. The QPO in these sources is slightly anticorrelated with energy (in Cyg X-1) or constant (in GS 2000+25). This is quite a different energy dependence than observed in the QPO of GX 339−4 and GS 1124−68 (see Tables 5 and 3, which are always spectrally hard). In particular, observations 1, 2, and 3 of GS 1124−68, which have spectral hardness similar to Cyg X-1 and GS 2000+25 here, are not spectrally flat or soft, but spectrally hard. This may imply a different mechanism for these QPOs of Cyg X-1 and GS 2000+25 from those of GS

TABLE 6

QPO PARAMETERS FOR GS 2000+25

	QPO			
ENERGY RANGE (keV)	ν_c (Hz)	FWHM (Hz)	rms (%)	χ^2_ν (dof)
2.3–4.6	...	...	...	3.40 (29)
	$2.41^{+0.15}_{-0.09}$	$1.3^{+0.6}_{-0.3}$	$4.9^{+1.3}_{-0.7}$	0.79(26)
4.6–9.2.....	(2.63)	(1.68)	5.6 ± 0.7	1.52 (28)
9.2–18.4	(2.63)	(1.68)	$5.4^{+1.3}_{-1.7}$	1.91 (30)
2.3–18.4	2.63 ± 0.06	1.7 ± 0.2	6.3 ± 0.5	1.39 (26)

NOTES.—Fit is of single observation period with wide *ratio* = 0.09–0.1. Values in parenthesis are fixed. Fits applied to values in the 0.125–8.0 Hz range.

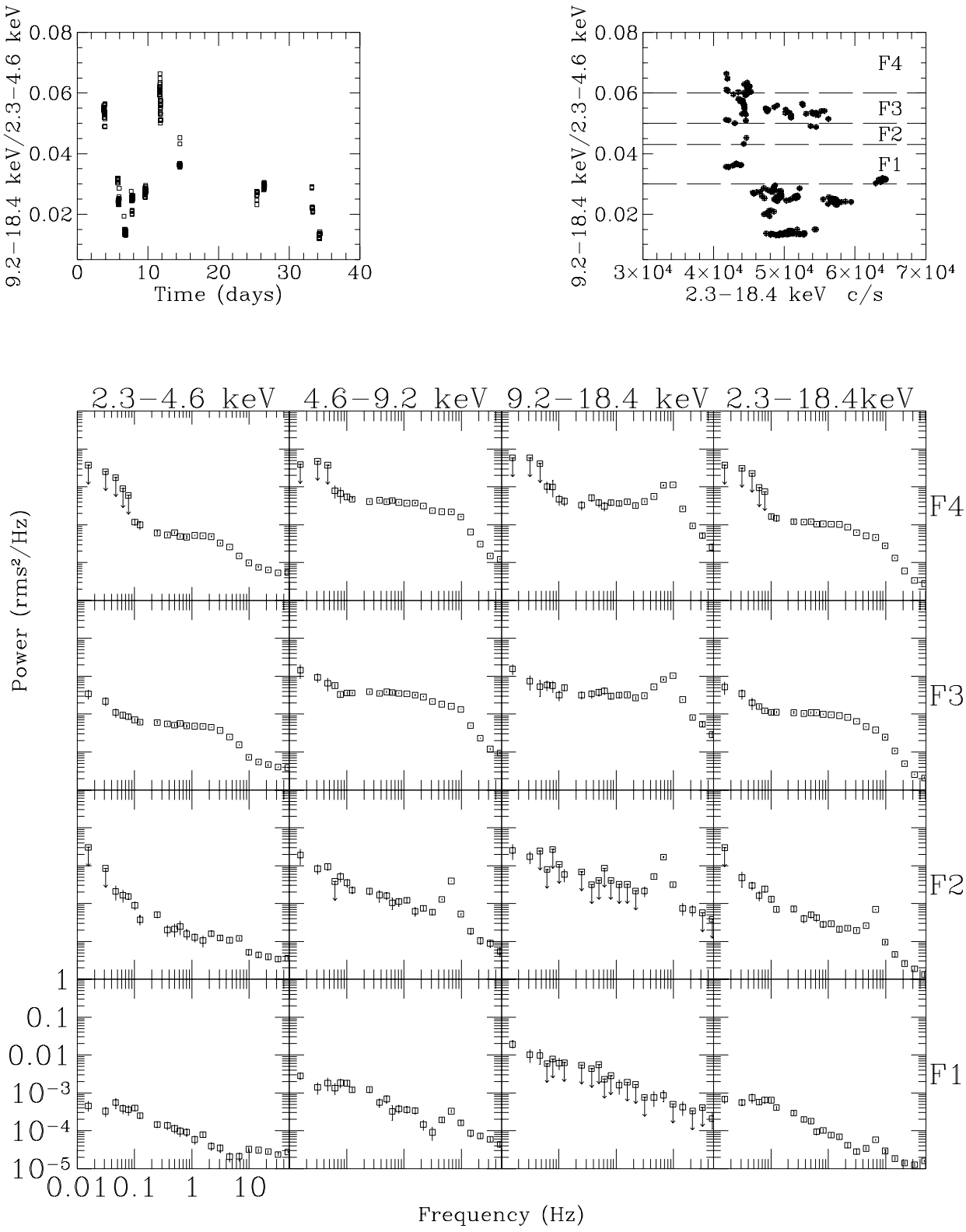

FIG. 7.—Detailed HID and PDS of GS 1124−68 with QPOs. (*Upper left panel*) Wide ratio vs. time, during the first 40 days of outburst. (*Upper right panel*) HID, intensity range count rate vs. wide ratio. The panel has been divided identically to Fig. 6 by wide ratio value, and each region is labeled. (*Bottom panels*) PDS in three energy ranges plus the intensity range (labeled by column) of the 1988 September observations. Upper limits are 2 σ. The data were divided by spectral hardness (each row is labeled, and corresponds to a label in the HID above). The BBN PDS characteristics evolve—as the spectrum softens, the BB PDS changes from a flat-top power law to a pure power law, while the QPO remains throughout.

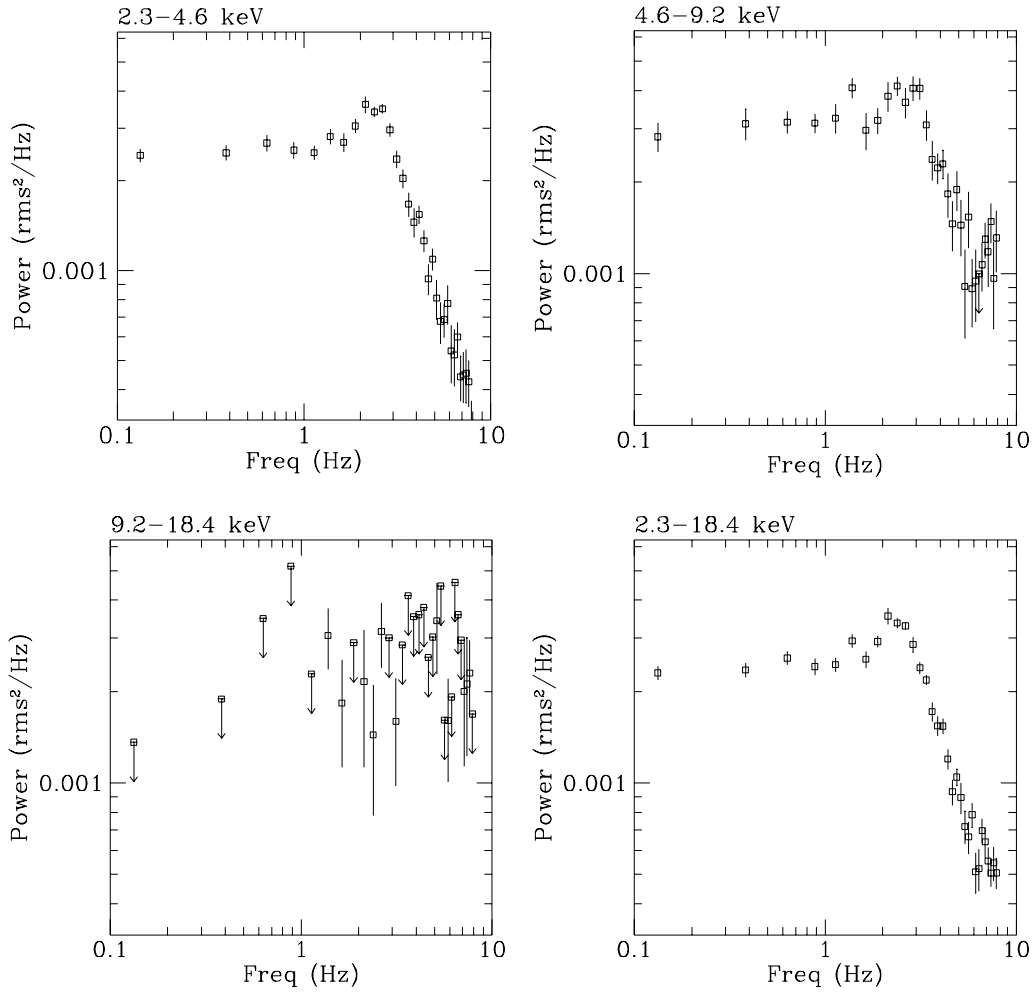

FIG. 8.—GS 2000+25 PDS of state with QPOs. The PDS in the three energy ranges and the sum energy range (indicated in each panel). Corrections for background and dead time have been applied to the Power. Upper limits are 2 σ.

1124−68 and GX 339−4. (We are unable to characterize the LS QPO of GX 339−4 reported previously by Grebenev 1991, as no information on the energy dependence of the variability is available).

3.4. *The Variability Ratio*

To compare the spectrum of the QPO relative to that of the broadband variability in the sources Cyg X-1, GS 2000+25, GX 339−4, and GS 1124−68, we define the variability ratio:

$$R_{\mathrm{QPO,BB}} = \frac{\%\mathrm{rms}_{\mathrm{QPO}}(9.2-18.4\mathrm{keV})}{\%\mathrm{rms}_{\mathrm{QPO}}(2.3-4.6\mathrm{keV})} \Big/ \frac{\%\mathrm{rms}_{\mathrm{BB}}(9.2-18.4\mathrm{keV})}{\%\mathrm{rms}_{\mathrm{BB}}(2.3-4.6\mathrm{keV})}, \quad (1)$$

which is a ratio of two ratios, each being the ratio of the high-energy range percent rms variability to the low-energy range percent rms variability, in the QPO and (separately) the broadband components. Values of the variability ratio which are consistent with 1.0 mean the QPO and BBN components have the same energy spectrum; values which are greater than 1.0 mean the QPO is spectrally harder than the BBN component. The variability ratio is independent of the source spectrum, in the sense that if the spectrum changes while the percent rms variability as a function of frequency remains the same, the variability ratio also remains the same.

For GS 2000+25 and Cyg X-1, the spectrum of the QPO is the same as, or slightly softer than the spectrum of the BBN variability. The variability ratio of GX 339−4 is significantly higher, which indicates that the VHS QPO is spectrally harder than the BBN variability. The same is often true for GS 1124−68: the VHS QPO is spectrally harder during observations 1, 3, 5, 10, and 11b. During observations 2, 8, and 15, however, the QPO spectral hardness is within a factor of 2 (spectrally harder) of the spectral hardness of the BBN variability.

In Figure 12, we show the variability ratio as a function of the wide ratio, for the four objects from which we identify QPOs. For GS 1124−68 and GX 339−4, the value of the ratio is high ($\gtrsim$4) while the wide ratio is in the range 0.03−0.08. While GX 339−4 was not observed with QPO outside of this range, GS 1124−68 was observed with spectral hardness both above and below this range, where the ratio is observed to be low ($\lesssim$2). For Cyg X-1 and GS 2000+25, from which QPO were observed in their LS, the value of the ratio was observed to be low ($\lesssim$2). The similarity in the value of the ratio observed from GS 1124−68, Cyg X-1, and GS 2000+25 while they have similar spectral hardness supports the argument that the QPO of these objects are of similar origin. The QPO centroid frequencies

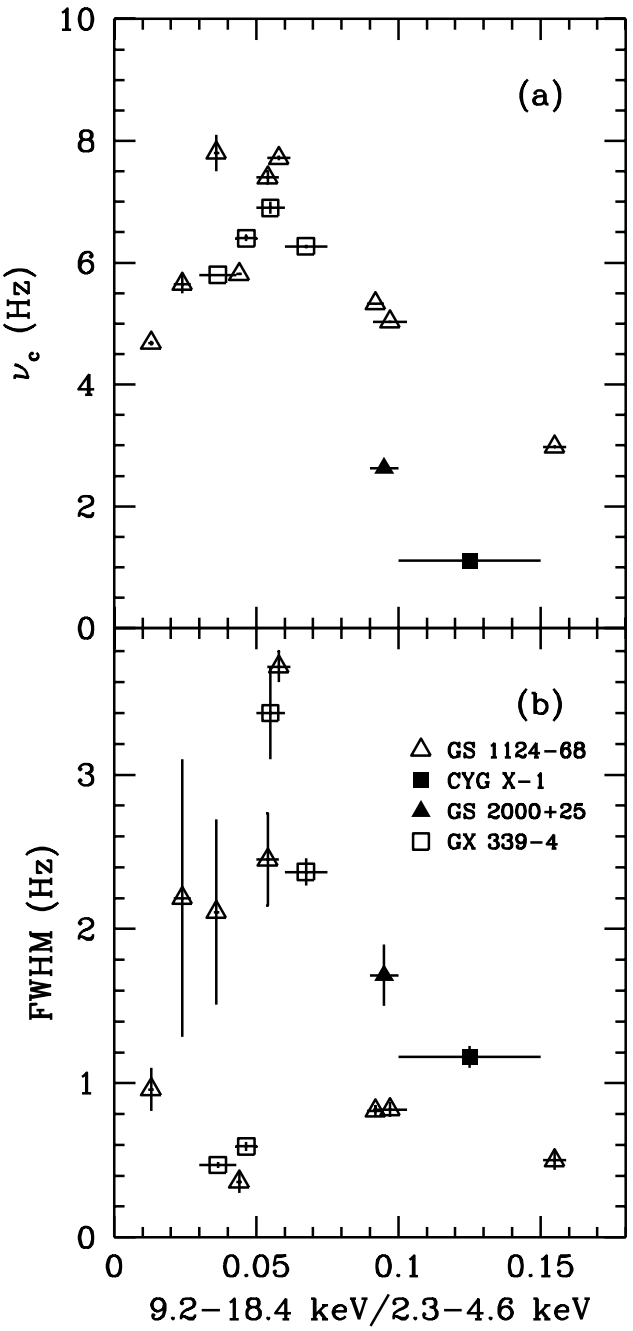

FIG. 9.—QPO centroid frequency (ν_c) and FWHM vs. wide ratio. (*a*) Centroid frequency of the fundamental QPO, as a function of wide ratio. Centroid frequency is maximum near wide ratio = 0.055. (*b*) FWHM of the fundamental vs. wide ratio. The FWHM is greatest near wide ratio = 0.055. 1 σ error bars are included on all points. The Cyg X-1 G2-data are not depicted (due to their high wide ratio) but follow these trends.

of GS 1124−68 were 3–5 Hz (observations 1–3; Tables 4 and 5), which are low, but not identical to the ~1 Hz frequencies of Cyg X-1 and GS 2000+25. Figure 13 illustrates the correlation between the variability ratio and the QPO centroid frequency measured from these sources.

4. DISCUSSION AND CONCLUSIONS

4.1. *Wide Ratio of BHCs when QPOs Are Observed*

While there is no simultaneous spectral data for the 6 hour observation period during which 0.08 Hz QPOs were found in LMC X-1 (Ebisawa, Mitsuda, & Inoue 1989), in the 13 hr following this period (observed with 16 s time resolution), the wide ratio was in the range 0.033–0.087 (Fig. 1) which is very close to the wide ratio of GS 1124−68 and GX 339−4 when QPOs were observed. Although high-frequency PDS were produced by Ebisawa et al., no 3–10 Hz QPOs were reported. However, the QPOs can turn on and off on a timescale of ≈1 s (Miyamoto et al. 1991; Takizawa et al. 1997), correlated with a sudden change in source spectral hardness (and intensity—the "flip-flops"), and this may explain the absence of QPO in LMC X-1.

We conclude that we observe no BHCs with spectral hardness $0.02 \lesssim$ wide ratio $\lesssim 0.1$ that do not exhibit QPO; consequently, we expect that BHCs with spectral hardnesses in this range should produce QPO similar to that described here.

4.2. *The Very High State as a Transition between the Low State and the High State*

Previous investigations using the present data concluded that both band-limited noise variability behavior (like that seen in the low state) and power-law noise variability (like that seen in the high state) are observed at various times simultaneous with QPO in GX 339−4 (Miyamoto et al. 1991) and GS 1124−68 (T97). In both studies, it was shown that these behaviors are observed when the object was relatively spectrally hard (in the case of low state–like noise) and spectrally soft (in the case of high state–like noise). Neither investigation commented upon the relationship between this transition and the expected transition between the low and high states.

In GS 1124−68 (T97), it was also found that the QPO centroid frequency had (at least) two distinct functional dependencies on the 2–20 keV intensity, one which was valid when power-law (HS-like PDS) variability was observed (in observations 11 and 15), the other when band-limited (LS-like PDS) variability was observed. Comparison with the present results shows that the change in the dependence of QPO frequency on intensity observed by T97 occurs at wide ratio ~0.055 ("the transition point").

1. The very high state of GX 339−4 and GS 1124−68 (i.e., when QPOs are observed) is spectrally between the low state and high state ($0.02 \lesssim$ wide ratio $\lesssim 0.2$);
2. Power-law PDS, similar to that expected from the spectrally soft high state, are observed when QPOs are present in both GX 339−4 and GS 1124−68 when these sources are spectrally softer than at the transition point ($0.02 \lesssim$ wide ratio $\lesssim 0.055$); in addition, the QPO centroid frequency is correlated with spectral hardness in this spectral region;
3. Band-limited PDS, similar to that expected from the spectrally hard high state, are observed when QPOs are present in both GX 339−4 and GS 1124−68 and when these sources are spectrally harder than at the transition point ($0.055 \lesssim$ wide ratio $\lesssim 0.2$); in addition, the QPO centroid frequency is anticorrelated with spectral hardness in this spectral region;

For the reasons listed above, it seems natural to interpret the VHS as the transition between accretion dominated by the spherical corona (the low state) and accretion dominated by the accretion disk (the high state). The change at

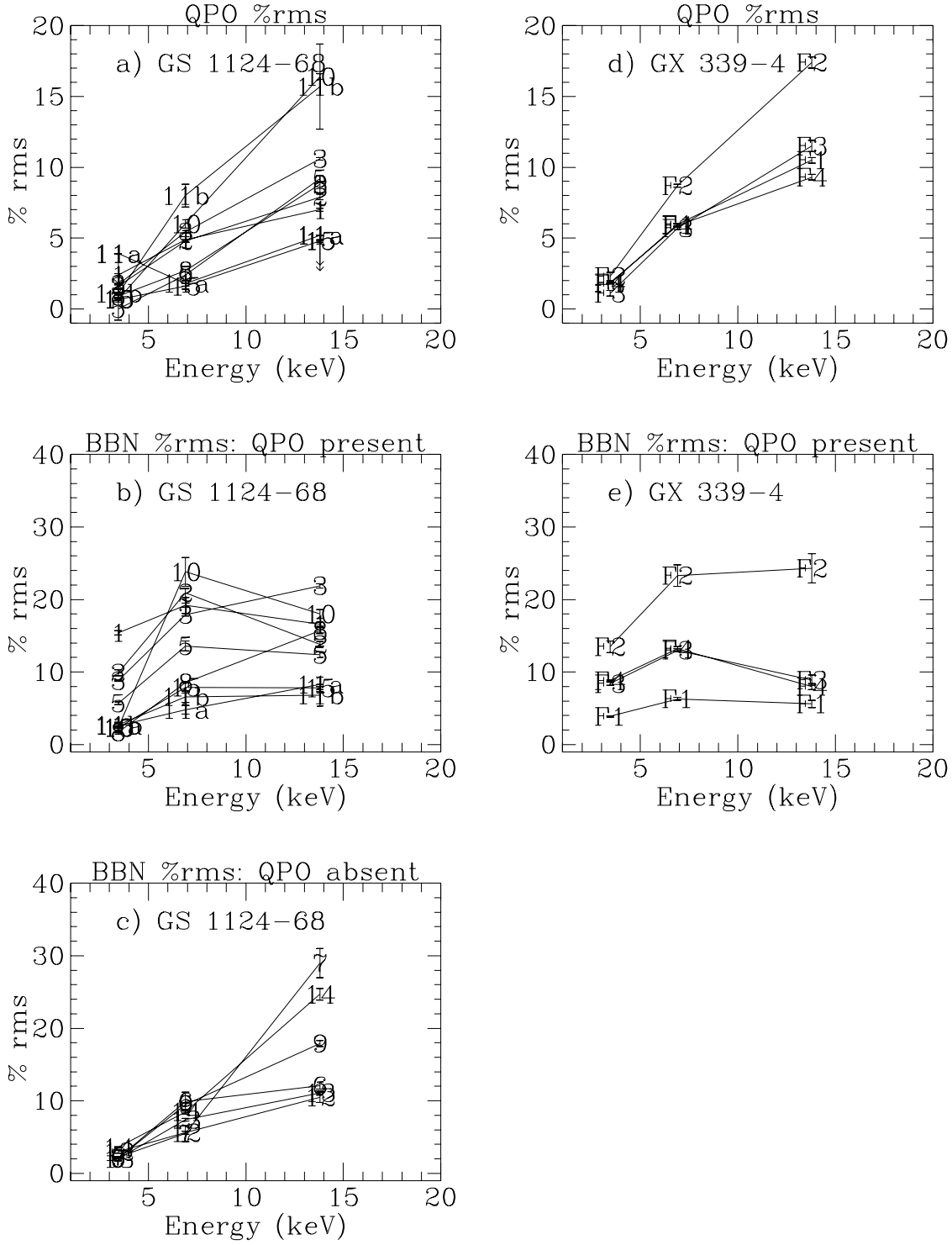

FIG. 10.—QPO and BBN percent rms, VHS QPO of GS 1124−68 & GX 339−4. The percent rms variability in the QPO and BBN components when QPO is present or absent, in GS 1124−68 and GX 339−4. Upper limits are 3 σ. Points for GS 1124−68 are marked with observation IDs from Table 4; points from GX 339−4 are marked with spectral indicator IDs taken from Fig. 6 (*a*) QPO percent rms vs. energy range from GS 1124−68. (*b*) BBN percent rms (when QPO is present) vs. energy range from GS 1124−68. (*c*) BBN percent rms (when QPO is absent) vs. energy range from GS 1124−68. (*d*) QPO percent rms vs. energy range from GX 339−4. (*e*) BBN percent rms (when QPO is present) vs. energy range from GX 339−4.

the (so-defined) transition point in the QPO spectral hardness relative to the BBN variability, as well as the dependence of the QPO centroid frequency on the wide ratio from a correlation to an *anti*correlation, may indicate that the QPO is a manifestation of the interaction between the corona and the accretion disk.

It is widely assumed that the accretion rate ($\dot{M}$) is correlated with the observed flux in BHCs and that the 2–20 keV flux is used as a monotonic indicator of this; thus, $\dot{M}$ increases monotonically from off state, to LS, to IS, to HS, to VHS (cf. Esin et al. 1997). Our results show that, when a BHC evolves between LS and HS, it should cross the spec-

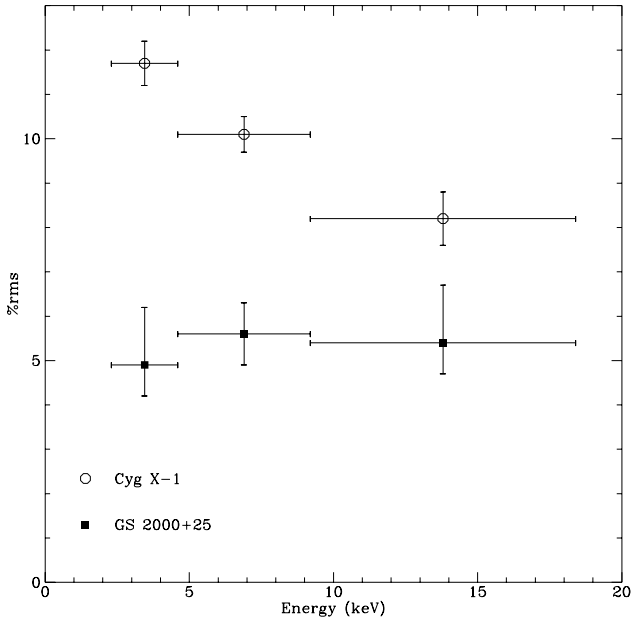

FIG. 11.—Percent rms of low-state QPO vs. energy range, Cyg X-1 and GS 2000+25. Cyg X-1 (*open circles*) and GS 2000+25 (*solid squares*) Error bars on the percent rms are 1 σ, while on energy they represent the energy range of the PDS. The QPO percent rms is soft (in Cyg X-1), and flat (in GS 2000+25). This contrasts with QPO in GS 1124−68 which, in the same spectral range (observations 1–3), as well as in all other observations and in GX 339−4 as well, is spectrally hard.

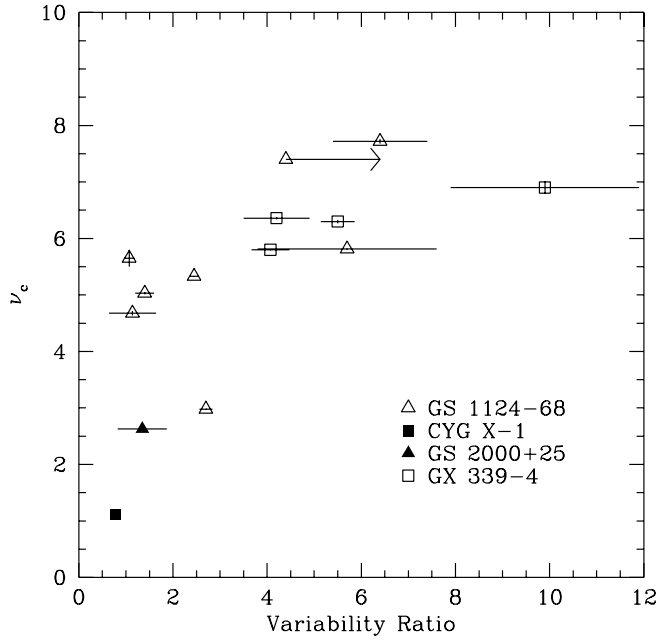

FIG. 13.—Variability ratio vs. QPO centroid frequency. The normalized ratio of QPO percent rms (eq. [1]) vs. the QPO centroid frequency of sources in the present study. A variability ratio of X indicates the QPO is X times as strong relative to the BBN variability in the high-energy range as it is in the low-energy range.

tral region in which we observe the VHS (being intermediate to the two) and that while doing so, the noise properties of the BHC should change from band limited to power law. This has been observed recently: Cyg X-1 exhibited 3–12 Hz QPOs during its 1996 transition, when its 2–20 keV intensity was between that of observed HS and LS (Cui et al. 1997) and GRO J1655−40, which exhibited 6.5 and 0.8 Hz QPOs (Méndez et al. 1998).

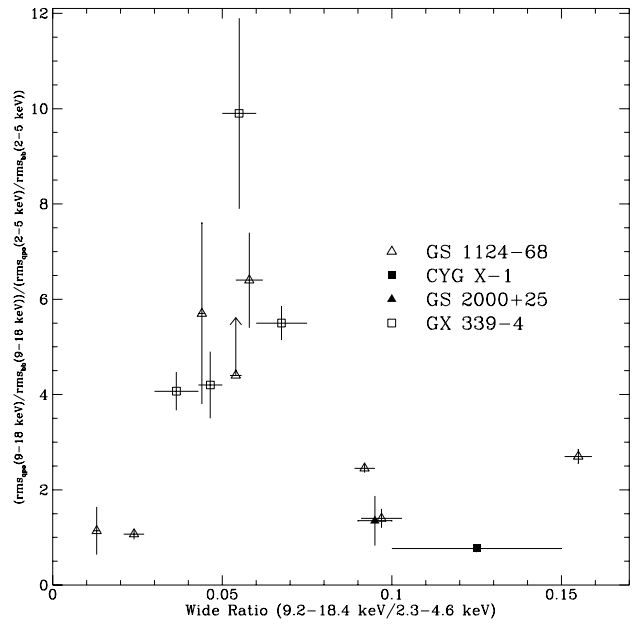

FIG. 12.—Variability ratio vs. spectral hardness. The variability ratio of QPO percent rms (eq. [1]) as a function of wide ratio, from the four QPO sources in the present study. A variability ratio of X indicates the QPO is X times as strong relative to the BBN variability in the high-energy range as it is in the low-energy range.

While Cyg X-1 underwent its 1996 transition, QPOs (of a broad type, $Q \approx 1$) were observed, with centroid frequencies between 3–12 Hz (Cui et al. 1997). In Figure 14, we show the dependence of Cyg X-1 QPO ν_c versus spectral hardness (from Tables 2 and 3 of Cui et al. 1997 and W. Cui 1998, private communication). The hardness ratio of 13.1–60 keV/2.0–6.5 keV was measured by *RXTE*/PCA and cannot be directly compared to the wide ratio measured by *Ginga*, although we can reasonably expect that the two are monotonically related.

Those observations with hardness ratio greater than 0.11 had a type of band-limited noise, with a power-law slope ~0.3–0.8 below ~0.5 Hz, then constant between ~0.5–2.0 Hz, breaking again into a power law of slope ~2.0 above that; during this period (called the "transition phase" by Cui et al.) the QPO centroid frequency was anticorrelated with spectral hardness. During those observations with hardness ratio less than 0.11 (called "soft state" by Cui et al.) the source variability was described as a broken power law (of slopes ~1 and 2, breaking near $\nu \sim 5$–15 Hz); in addition, the QPO centroid frequency was below that observed in the softest (but relatively spectrally harder) "transition phase" observations, indicating an anticorrelation with spectral hardness.

Comparison between the dependence on the QPO centroid frequency in Cyg X-1 (Fig. 14) with that of GX 339−4 and GS 1124−68 (Fig. 9*a*) shows that in all three objects, the centroid frequency is correlated with spectral hardness, which changes to an *anti*correlation above some spectral hardness; in addition, all three objects show power-law PDS behavior when the centroid frequency is correlated with spectral hardness, and band-limited PDS behavior

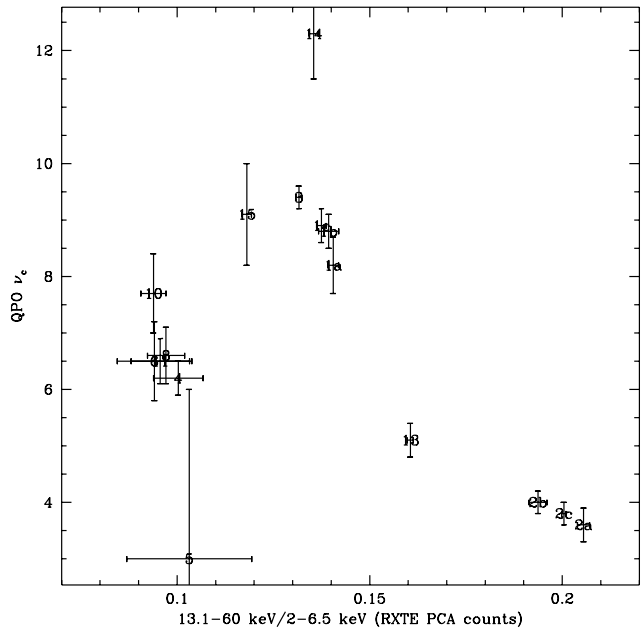

FIG. 14.—Cyg X-1 1996 transition, QPO centroid frequency vs. spectral hardness. The ν_c-values are taken from Tables 2 and 3 of Cui et al. (1997), and spectral hardnesses by W. Cui (1998, private communication). The value of the spectral hardness ratio is as measured by *R*XTE/PCA and cannot be directly compared to the wide ratio measured by *Ginga* although the spectral hardness is monotonic, and so can be qualitatively compared to the ν_c vs. wide ratio of GX 339−4 and GS 1124−68 (Fig. 9). Each point is marked with the observation number taken from the table of Cui et al. (1997).

when the centroid frequency is anticorrelated with spectral hardness.

The differences between the behavior of Cyg X-1 and that which we observe from GX 339−4 and GS 1124−68 is that the QPOs (in Cyg X-1) are considerably broader QPOs ($Q \approx 1$ compared with $Q \approx 10$), and the 2–20 keV flux is only moderately greater than its low state flux and still below that of its high state (Belloni et al. 1997), while GX 339−4 and GS 1124−68 were observed with ~2–20 keV intensities greater than periods where "high state" behavior was observed. It was on the basis of this discrepancy in 2–20 keV intensity in Cyg X-1 (Cui et al. 1997), as well as during a period when QPOs were observed at low intensity in GS 1124−68 (Belloni et al. 1997), that analogy with the VHS was discarded. However, the change in dependence of the QPO centroid frequency on spectral hardness, associated with the change in the BBN variability is suggestive that the phenomena of Cyg X-1 observed during transition between low and high state is the same as that which we describe of GS 1124−68 and GX 339−4 in their VHS, in spite of the differences in ~2–20 keV intensity.

We conclude that the conditions for transition between the two states occur at luminosities both above (in the case of the VHS) and below (in the case of the IS) the high state in BHCs.

We cannot exclude that the assumption that the 2–20 keV flux (usually thought to correspond to $\dot{M}$) is a monotonic indicator of states is not correct. For example, GS 2023+33 exhibited spectral and timing behavior which has been classified as "low state" (spectrally hard, with band-limited noise), even at its highest luminosity—although much caution must be employed in interpreting this behavior, as GS 2023+33 was a peculiar X-ray transient in more than one way (cf. Tanaka & Lewin 1995).

The strength of the underlying BBN variability is (in GS 1124−68) on average decreased by the presence of QPOs. One might interpret this to mean that, while the physical process producing the VHS QPO is distinct from that of the BBN variability, there is nonetheless interaction between the two processes which affects the strength of the BBN variability.

It does not follow naturally from any other observed behavior that, as a function of spectral hardness, the variability ratio should be low (~1), *increase* with increasing spectral hardness toward the transition point (wide ratio ~0.055, where it is $\gtrsim 4$), and then *decrease* with increasing spectral hardness. This therefore represents a significant and interesting phenomenon, which requires further discussion. It implies that the spectrum of the QPO is (in the low state) similar to the spectrum of the BBN variability; as the source spectrum evolves toward the high state, the QPO spectrum becomes spectrally hard, relative to the BBN variability, becoming maximally spectrally hard relative to the BBN variability at the same wide ratio as when the QPO centroid frequency is at its maximum; and then, as the spectrum evolves further toward the high state, the spectrum of the QPO again softens toward the spectrum of the BBN variability. (We emphasize here that "evolution" is as a function of spectral hardness, not of time). There exists no a priori reason that the QPO photon spectrum should at any time be in any way similar to the BBN variability photon spectrum—the variability ratio could, in principle, take on any value between 0 and infinity. That the lowest observed values of the variability ratio indicate that the QPO energy spectrum is similar to the BBN energy spectrum suggests that the QPO itself is due to the same mechanism as the BBN variability, which for some unknown reason becomes enhanced at a particular frequency.

In summary, the observed dependence on spectral hardness of the BBN variability while QPOs are observed from GX 339−4 and GS 1124−68 and their position on the color-color diagram spectrally intermediate to the low state and high state indicate that the so-called VHS QPO is due to interaction between the physical component responsible for low-state behavior and that responsible for high-state behavior. Our comparison with QPOs observed from Cyg X-1 at lower luminosity, during transition between the low and high states, indicate that these QPOs may also be due to such interaction. If this inference is correct, then the QPOs may prove a useful probe in investigating the properties of the interaction of the different accretion components in BHCs.

R. R. is grateful to W. Cui for providing the unpublished spectral hardness ratios measured from Cyg X-1. R. R. is also grateful to L. Bildsten for his hospitality at UC Berkeley where this work was completed. T. O. acknowledges an ESA Research Fellowship. M. K. gratefully acknowledges the Visiting Miller Professor Program of the Miller Institute for Basic Research in Science (UCB). W. H. G. L. acknowledges support from NASA.

REFERENCES

Abramowicz, M. A., Chen, X., & Taam, R. E. 1995, ApJ, 452, 379
Belloni, T., Méndez, M., van der Klis, M., Hasinger, G., Lewin, W. H. G., & van Paradijs, J. 1996, ApJ, 472, L107
Belloni, T., van der Klis, M., Lewin, W. H. G., van Paradijs, J., Dotani, T., Mitsuda, K., & Miyamoto, S. 1997, A&A 322, 857
Chen, X., Abramowicz, M. A., Lasota, J.-P., Narayan, R., & Yi, I. 1995, ApJ, 443, L61
Chen, X., & Taam, R. E. 1996, ApJ, 466, 404
Cui, W., Zhang, S. N., Focke, W., & Swank, J. H. 1997, ApJ, 484, 383
Ebisawa, K. 1991, Ph.D. thesis, Univ. Tokyo
Ebisawa, K., Mitsuda, K., & Inoue, H. 1989, PASJ, 41, 519
Esin, A. A., McClintock, J. E., & Narayan, R. 1997, ApJ, 489, 865
Grebenev, S. A., Siuniaev, R. A., Pavlinskii, M. N., & Dekhanov, I. A. 1991, Soviet Astron. Lett., 17, 985
Hasinger, G., & van der Klis, M. 1989, A&A, 225, 79
Liang, E., & Narayan, R. 1997, in AIP Conf. 410, Proc. Fourth Compton Symp. ed. C. D. Dermer, M. S. Strickman, & J. D. Kurfess (New York: AIP), 461
Makishima, K., Maejima, Y., Mitsuda, K., Bradt, H. V., Remillard, R. A., Tuohy, I. R., Hoshi, R., & Nakagawa, M. 1986, ApJ, 308, 635
Méndez, M., Belloni, T., & van der Klis, M. 1998, ApJ, 499, L187
Méndez, M., & van der Klis, M. 1997, ApJ, 479, 926
Mitsuda, K., et al. 1984, PASJ, 36, 741
Miyamoto, S., Iga, S., Kitamoto, S., & Kamado, Y. 1993, ApJ, 403, L39
Miyamoto, S., Kimura, K., Kitamoto, S., Dotani, T., & Ebisawa, K. 1991, ApJ, 383, 784
Miyamoto, S., Kitamoto, S., Iga, S., Hayashida, K., & Terada, K. 1994, ApJ, 435, 398
Narayan, R. 1996, ApJ, 462, 136
Narayan, R., & Yi, I. 1994, ApJ, 428, L13
———. 1995, ApJ, 452, 710
Press, W., Flannery, B., Teukolsky, S., & Vetterling, W. 1995, Numerical Recipies in C (Cambridge: Cambridge Univ. Press)
Rutledge, R., Lewin, W. H. G., Dotani, T., Mitsuda, K., van Paradijs, J., Vaughan, B., & Klis, M. V. D. 1999, in preparation (BHCLFN)
Rutledge, R. E. 1996, Ph.D. thesis, MIT
Takizawa, M., et al. 1997, ApJ, 489, 272 (T97)
Tanaka, Y., & Lewin, W. 1995, in X-Ray Binaries, Vol. 1, ed. W. Lewin, J. van Paradijs, & E. Van Den Heuvel (Cambridge: Cambridge Univ. Press), 126
Turner, M., et al. 1989, PASJ, 41, 345
van der Klis, M. 1994a, A&A, 283, 469
———. 1994b, ApJS, 92, 511
———. 1995a, in X-Ray Binaries, Vol. 1, ed. W. Lewin, J. van Paradijs, & E. Van Den Heuvel (Cambridge: Cambridge Univ. Press), 252
van Paradijs, J. 1995b, in X-Ray Binaries, Vol. 1, ed. W. Lewin, J. van Paradijs, & E. Van Den Heuvel (Cambridge: Cambridge Univ. Press), 536